American Mineralogist, Volume 111, pages 360–375, 2026

Infrared spectroscopy of natural *Type Ib* diamond: Insights into the formation of *Y*-centers and the early aggregation of nitrogen

Maxwell C. Day[1,*,‡,§], Michael C. Jollands[2], Francesca Innocenzi[1], Davide Novella[1], Fabrizio Nestola[1,†], and Martha G. Pamato[1]

[1]Dipartimento di Geoscienze, Università degli Studi di Padova, Via Gradenigo 6, 35131 Padova, Italy
[2]Gemological Institute of America (GIA), 50 W 47th Street, New York, New York 10036, U.S.A.

Abstract

The growing interest in the spectroscopic properties of *Type Ib* diamonds has revealed several complexities associated with nitrogen (N)-related defects that have yet to be identified. One defect in particular, the ***Y***-center, produces a characteristic spectrum in the N-region (~1000–1400 cm^{-1}) that is extremely common in the IR spectra of diamonds with a dominant *Type Ib* component. In this study, a suite of 178 *Type Ib* + *IaA* diamonds with variable N-aggregation states (%IaA) and N contents was examined to evaluate the effect of ***Y***-center absorbance on the results obtained from standard deconvolution of the N-region. To achieve this, a new deconvolution routine was developed that incorporates the ***Y***-center spectrum (obtained by decomposition of *Type Ib* spectra), and an updated spreadsheet (*Caxbd_Inherit_2024-Ib*, Online Materials[1]) for processing the IR spectra of *Type Ib* diamonds is provided here. It is shown that neglecting ***Y***-center absorption during least-squares fitting of the IR spectra of *Type Ib* + *IaA* diamonds results in poor-quality fits of the N-region that may result in erroneous ***C***- and ***A***-center contents. The identity of the ***Y***-center, and the relevant absorption coefficient, have not been constrained. However, several studies have shown that ***Y***-centers are structurally related to single-substitutional N (called N_S^0 or ***C***-centers); thus, the ***Y***-center contents were calculated using the ***C***-center absorption coefficient. Using the new deconvolution method, it is shown that neglecting ***Y***-centers may result in N-aggregation states that vary by ±10 %IaA and total N contents (N_{tot}) that may be overestimated by >100 at. ppm. The samples studied here have an average N_{tot} of ~100 at. ppm, and errors in %IaA and N_{tot} may be much larger for diamonds with higher N_{tot}. Such errors translate to potentially significant discrepancies in the calculated mantle residence times on the order of hundreds of millions of years. Comparisons of the normalized ***Y***-center content and %IaA show that ***Y***-centers are an intermediate defect that is produced from 0 to 40 %IaA at the expense of ***C***-centers and then consumed from 40–100 %IaA to produce ***A***-centers. A strong linear correlation with some IR peaks between 1400 and 1350 cm^{-1} (e.g., 1358 cm^{-1}) is observed. Evidence supporting the assignment of such peaks to defects containing interstitial carbon and nitrogen (C_i and N_i) is described, suggesting that the formation of ***Y***-centers is driven by interstitial-assisted aggregation. Moreover, the ***Y***-center itself may be an intermediate form of N_S^0 linked to C_i or N_i or larger interstitial complexes that become unstable with increasing N-aggregation (mantle residence time/temperature). Evidence for alternative hypotheses for the identity of the ***Y***-center involving O- and Ni-related defects and ***X***-centers is also discussed.

Keywords: Diamond, *Type Ib* diamond, FTIR spectroscopy, defects, N-aggregation, substitutional nitrogen, ***Y***-centers, Spectroscopy in geology: a decade of breakthroughs

Introduction

The study of impurities in diamond, particularly nitrogen (N), which forms substitutional and interstitial defects, provides important information about the composition of mantle substrates and the sources of fluids/melts associated with diamond formation (Shatsky et al. 2014; Reutsky et al. 2017; Zedgenizov et al. 2017; Curtolo et al. 2023; Day et al. 2023). Nitrogen is the most abundant impurity observed in natural diamonds, and a tremendous amount of work has been aimed at understanding the mechanisms and rates of N-defect migration and aggregation (Evans and Qi 1982; Mainwood 1994; Taylor et al. 1996; Jones et al. 2015). In *Type Ib* diamond, N occurs predominately as single-substitutional atoms in the neutral charge-state (N_S^0) called ***C***-centers. With continued annealing, ***C***-centers aggregate to form N_2 defects (a pair of substitutional N atoms called ***A***-centers) in *Type IaA* diamonds and eventually *V*N_4 defects, four substitutional N atoms surrounding a carbon (C) vacancy (*V*) called ***B***-centers, in *Type IaB* diamonds (Evans and Qi 1982; Taylor et al. 1996; Kiflawi et al. 1997). Deconvolution of the unique signal produced by each of these defects in the one-phonon region (i.e., N-region) allows calculation of the N-aggregation state, i.e., A/(C + A) × 100 = %IaA or B/(A + B) × 100 = %IaB, where C, A, and B represent the concentration of N (in at. ppm) in ***C***-, ***A***- and ***B***-centers. Moreover, the time/temperature dependence of the idealized aggregation sequence ***C*→*A*→*B*** has been

* Corresponding author E-mail: maxwell.day@unipd.it Orcid https://orcid.org/0000-0002-3295-2116
† Orcid https://orcid.org/0000-0002-4875-5125
‡ Special collection papers can be found online at our website in the Special Collection section.
§ Open access. Article available to all readers online under the following license terms: CC BY.

0003-004X/26/0003–360$05.00/DOI: https://doi.org/10.2138/am-2024-9722

Downloaded from pubs.geoscienceworld.org/msa/ammin/article-pdf/111/3/360/7778962/ammin-2025-9722.1.pdf by guest on 30 October 2026

determined experimentally, and thus the N-aggregation state of a diamond can be used to estimate the time or temperature (if one or the other is known/assumed) of diamond residence in the mantle post-formation and pre-eruption (Taylor et al. 1990; Mendelssohn and Milledge 1995; Day et al. 2023).

However, the ***C→A→B*** aggregation sequence in reality is much more complex. The migration and eventual aggregation (combination) of N-related defects is driven by: (1) vacancy- and/or (2) (self-)interstitial-assisted aggregation sequences involving *V* and interstitial carbon (i.e., a self-interstitial, C_i) and nitrogen (i.e., an interstitial, N_i) and, in some cases, other interstitials like nickel (Ni) and cobalt (Co) (Collins 1980; Kiflawi et al. 1998; Jones et al. 2015). These are associated with different migration/formation mechanisms and activation energies (E_a) for different defects that control the rate of defect formation (e.g., ***C→A*** aggregation rate) (Mainwood 1994; Taylor et al. 1996). The ***C→A*** aggregation sequence also involves intermediate defects that correspond to discrete phases of N-aggregation (i.e., the transformation of ***N1***-centers [N-C-N defect] to ***A***-centers, Nadolinny et al. 2024) and/or N-defects with electronic properties that differ from the traditional ***C***- and ***A***-centers (i.e., positively charged single-substitutional N_S^+ defects called ***X***-centers) (Lawson et al. 1998). The growing body of evidence for different N-related defects (e.g., Dischler 2012; Ashfold et al. 2020), supported largely by spectroscopic data, has resulted in the proposition of novel N-aggregation sequences that may involve volatile impurities, such as hydrogen (H) (Goss et al. 2002; Massi 2006; Wood 2020; Day et al. 2024), transition-metal impurities, including Ni and Co (Fisher and Lawson 1998; Nadolinny et al. 2000), and a large number of different (self-)interstitial complexes that involve interstitial C_i and N_i (Mainwood et al. 1978; Kiflawi et al. 1996; Goss et al. 2001, 2003; Liggins et al. 2010). The passivation of dangling carbon bonds by H has been shown to impede N-aggregation and drive the formation of *V*/N/H-related defects (e.g., VN_3H) through several different sequences (Goss et al. 2014; Peaker et al. 2015; Day et al. 2024). The formation of Ni-related defects leads to the production of C_i (Nadolinny et al. 2000) which has been shown to promote the formation of ***A***-centers (Kiflawi et al. 1997) and other related defects such as the ***H1a***-center (N_S^0 and N_i occupying one carbon site, Goss et al. 2004; Liggins et al. 2010) and the N_2V defect which in-turn, disassociate to form ***A***-centers with progressive annealing (Jones et al. 2015). The traditional ***C→A*** and ***A→B*** aggregation sequence has been shown to follow a second-order rate equation (Evans and Qi 1982; Mainwood 1994; Taylor et al. 1996) allowing for the calculation of mantle residence time/temperature for natural diamond. However, the involvement of impurities other than N (e.g., H and Ni as discussed above) may cause departures from the second-order kinetics that can produce large errors associated with calculated residence times/temperatures (Fisher and Lawson 1998; Jones et al. 2015). Moreover, evidence for the disaggregation of ***B***-centers (Kanda and Watanabe 1999; Nadolinny et al. 2020) and ***A***-centers (Kiflawi and Bruley 2000) suggests that some proportion of ***A***- or ***C***-centers may form from disaggregation (rather than aggregation) and will contribute to errors associated with %IaA or %IaB and thus residence times/temperatures.

Despite these potential sources of error, deconvolution of the infrared spectra of *Type IaA* and *IaB* diamonds often produces high-quality fits of the N-region, and the resultant N contents and residence temperatures are typically in reasonable agreement with chemical data from alternative techniques [e.g., secondary-ion mass spectrometry (SIMS)] and (elastic) thermobarometric data from analyses of mineral inclusions (e.g., Nestola et al. 2018; Kaminsky et al. 2024). This is because the degree to which alternative N-aggregation sequences (distinct from ***A→B***) are active decreases with progressive annealing (increasing residence times/temperatures). This has been observed in H-bearing diamonds, where a drastic decrease in the number of different *V*/N/H-related defects coincides with the progressive loss of ***C***-centers, producing *Type IaA* and eventually *Type IaB* diamonds (Day et al. 2024).

The case is much different for *Type Ib* and *Ib + IaA* natural diamonds that contain detectable amounts of both ***C***- and ***A***-centers (using standard FTIR spectroscopy). Deconvolution of the infrared spectrum of natural diamonds with a dominant *Type Ib* component (i.e., ≤50 %IaA), with the most commonly used software (e.g., DiaMap), often produces poor quality fits, and there is a growing body of evidence that suggests this is due to an N-related defect referred to as the ***Y***-center (Hainschwang et al. 2008, 2012; Titkov et al. 2008; Titkov et al. 2015a, 2015b; Zedgenizov et al. 2019; Mashkovtsev et al. 2021). Here, an important distinction must be made between natural and synthetic diamonds, as ***Y***-centers have not yet been reported in chemical vapor deposition (CVD) or high-pressure, high-temperature (HPHT) synthetic diamonds. Hainschwang et al. (2012), the first to definitively demonstrate the existence of ***Y***-centers, describe similarities between the ***F***-center absorption system described earlier by Clark and Davey (1984) in *Type Ib + IaA* diamonds, which is most likely representative of the same defect. Thus far, no structural model of the ***Y***-center has been proposed. However, the prevalence of plastic deformation features (e.g., amber centers) in *Type Ib* diamonds suggests that the formation of ***Y***-centers may require interstitial N_i and C_i (and/or *V*) produced during deformation and dislocations (Smit et al. 2018). A potential genetic relationship between ***Y***-center absorption and the 480 nm band (assigned to substitutional oxygen [O] and/or Ni-related defects) has been described (Hainschwang 2014; Kupriyanov et al. 2020; Lai et al. 2024). A different model for the ***Y***-center has been proposed, which involves an extended defect where electrons from ***C***-centers interact with distant ***X***-centers (Titkov et al. 2015a). However, direct evidence for this model has not yet been found. ***Y***-centers are associated with a broad peak centered at ~1145 to 1150 cm^{-1} and sharper characteristic peaks at 1220 to 1240 cm^{-1} and have been shown to produce significant residual intensity after fitting and deconvolution of the N-region using the spectra of ***C***- and ***A***-centers (Hainschwang et al. 2012). As the identity and absorptivity (i.e., μ1145–1150 cm^{-1} absorption coefficient) of ***Y***-centers remains unknown, it is not surprising they are often overlooked during deconvolution, as one must either accept errors in ***C***- and ***A***-center contents due to neglecting ***Y***-centers or choose not to process the spectra of any diamond with ***Y***-centers. Moreover, given that least-squares fitting of the N-region has been streamlined in programs such as DiaMap

Downloaded from pubs.geoscienceworld.org/msa/ammin/article-pdf/111/3/360/7778962/ammin-2025-9722.1.pdf by guest on 30 October 2026

(Howell et al. 2012b, 2012a), Caxbd_o2010 (De Beers UK Ltd, Maidenhead, 2010), and QUIDDIT (Speich and Kohn 2020), users may be less likely to evaluate trends in residual signal after batch processing of large numbers of spectra.

In this study, averaged (bulk) infrared spectra were recorded from 178 *Type Ib + IaA* diamonds and were processed using a new deconvolution routine allowing for the simultaneous derivation of the ***C***-, ***A***-, ***X***-, and ***Y***-center components of each spectrum. A diverse sample suite with variable %IaA, N content, and ***C***-, ***A***-, and ***X***-center content has allowed the assessment of the degree to which ***Y***-centers affect the results of deconvolution and, consequently, the accuracy of calculated mantle residence times and temperatures. Despite the limitations of bulk spectra, the large number of samples has allowed recognition of several important correlations between N-defect contents and normalized peak intensities. The determination of the ***X***- and ***Y***-center composition of each diamond has revealed new trends between several of the first-formed N-related defects and their relative concentrations at different N-aggregation states.

Terminology and Nomenclature

Each IR spectrum was processed using different deconvolution routines, and several of the resultant fitting and deconvolution values are discussed in a comparative manner. Moreover, spectral lines observed in the IR and their potential correspondence to a large number of different defects (with different structural and electronic properties) are discussed. Consequently, the following terminology was developed and is listed below for the purposes of clarity.

Type Classification

Each diamond is described with the modified Type Classification used by Day et al. (2024) (modified from Robert et al. 1933 and Hainschwang 2014). Here, the relative concentrations of ***C***-, ***A***-, and ***B***-centers are indicated in the *Type*, e.g., diamond 1 = *Type IaA > Ib* describes a diamond with more N in ***A***-centers (at. ppm) than in ***C***-centers. As all diamonds studied here contain variable amounts of ***X***- and ***Y***-centers, the corresponding symbols are not indicated in the Type classification. However, signal in the one-phonon region of some diamonds (see Discussion) is dominated by solely ***X***- and/or ***Y***-center absorption and, thus, described as *Type IbX*, *IbY*, or *IbXY* accordingly (Hainschwang 2014). In many cases, we broadly describe diamonds that contain different N-defects but do not specify their relative abundance, e.g., *Type IaA + Ib* describes a diamond with detectable amounts of both ***A***- and ***C***-centers.

N-Aggregation State

The specific N-aggregation state is always expressed as %IaA, as no diamonds studied here contain detectable ***B***-centers. The N-aggregation state determined using the conventional deconvolution routine [i.e., with DiaMap (Howell et al. 2012b, 2012a)] is indicated as %IaA. The N-aggregation state determined by incorporating the ***Y***-center spectrum during deconvolution (i.e., with the updated spreadsheet including ***Y***-centers, *Caxbd_Inherit_2024-Ib*, see Online Materials[1]) is indicated as %IaA(Y).

Different absorption bands due to different defects do not convolute but instead produce a composite signal, following the additivity principle. Therefore, decomposition, compared to deconvolution, more accurately describes the process by which component bands are isolated from the complex composite absorption. However, as the term "deconvolution" has become deeply ingrained in the community, we use it here for the sake of clarity.

N-Defect Content

The concentration (in at. ppm) of N associated with ***C***-, ***A***-, ***X***-, and ***Y***-centers determined by deconvolution with and without incorporation of the ***Y***-center spectrum are indicated as N_C, N_A, and N_X and $N_C(Y)$, $N_A(Y)$, $N_X(Y)$, and N_Y, respectively. Similarly, total N contents are given as N_{tot} and $N_{tot}(Y)$. Since samples show variable N_{tot}, it is useful to normalize $N_C(Y)$, $N_X(Y)$, and N_Y to N_{tot}, allowing for comparison. Normalized $N_C(Y)$, $N_X(Y)$, and N_Y values are expressed as %***C***(Y), %***X***(Y), and %***Y***, e.g., $\%\boldsymbol{Y} = 100 \times N_Y/N_{tot}$.

IR Absorption Peaks and Systems

Local (discrete) vibrational modes (LVMs) typically give rise to sharp IR peaks that are best defined (fit) with a single function. Absorption systems produce broad peaks over a much wider frequency range and are best defined (or fit) using multiple component functions. Relatively intense regions (peaks) in the different absorption systems are referred to as ***C***-, ***A***-, ***X***-, and ***Y***-center components. Their intensities (after baseline correction and thickness normalization) are used in conjunction with the appropriate absorption coefficient to calculate the concentration of the corresponding defect. Here, the normalized intensity (after baseline correction) of such peaks (or frequency regions) is indicated using their position (e.g., μ1130 cm^{-1} for ***C***-centers) such that their intensity can be compared independently of the concentration of the corresponding defect (e.g., N_C). For the ***Y***-center absorption system, the averaged thickness normalized intensity from 1145 to 1150 cm^{-1} (μ1145–1150 cm^{-1}) is used to calculate N_Y-center content (see "Methods and Materials" and Online Materials[1] Appendix A).

Impurities and Defects

Only a small proportion of spectral lines observed in diamond have been definitively assigned to specific defects, and the properties of only a handful of these defects have been rigorously determined. Consequently, if only the identity of the impurity (e.g., N or H) associated with a specific defect (and spectral line) is known, we simply refer to such a defect as *impurity*-related. For example, "N-related defect" (or "N-defect") indicates a defect that is thought to contain only N, and a "*V*/N-related defect" indicates a defect that may contain *V* and N. Where the identity of a defect is known or has been proposed, it is indicated normally, e.g., VN_2^0, and the name of defects (e.g., ***H3***-center) is indicated where the respective defect is discussed. Interstitial impurities are indicated with a subscript *i* (e.g., interstitial, N_i or self-interstitial, C_i) and (self-)interstitial complexes are described accordingly, e.g., (N_i-N_i) or (C_i-N_i). In Online Materials[1] Table C1, the names, identities, compositions, and identifying signals assigned to point and extended defects discussed in this paper are provided.

Downloaded from pubs.geoscienceworld.org/msa/ammin/article-pdf/111/3/360/7778962/ammin-2025-9722.1.pdf by guest on 30 October 2026

Methods and Materials

A set of FTIR spectra recorded from *Type Ib* + *IaA* diamonds with variable %IaA and total N-contents was selected from the Gemological Institute of America (GIA) database. All spectra were recorded from diamonds submitted to the GIA for gemological analysis; other spectroscopic data, their source locality, and any other identifying information (e.g., color or the presence of inclusions) were not provided for confidentiality reasons.

Fourier Transform Infrared (FTIR) Spectroscopy

FTIR spectra were recorded from *Type Ib* + *IaA* diamond samples at the GIA using a diffuse reflectance DRIFT accessory attached to Thermo Fisher Nicolet iS50 units equipped with a KBr beam splitter and a LN-cooled MCT detector. The spectra were recorded at an operating resolution of 1 cm^{-1} with 32 scans, over the range 6000–650 cm^{-1}. Additional spectra were recorded from one *Type Ib* diamond from the Zimmi locality (Smit et al. 2016) to test the assumed ***Y***-center absorption coefficient (see Online Materials[1] Appendix A). These spectra were collected at the University of Padova (Italy) using a Thermo Fisher Nicolet iN10 InfraRed microscope equipped with a KBr beam splitter and a LN-cooled MCT detector. The spectra were recorded at an operating resolution of 2 cm^{-1} with 64 scans over the range 6000–750 cm^{-1}. The deconvolution results for the Zimmi diamond were averaged from six spectra.

Before deconvolution, all spectra were baseline corrected (using polynomial fitting) and normalized to a *Type IIa* reference spectrum, following the procedure outlined in the DiaMap Excel spreadsheet (Howell et al. 2012b, 2012a). Initial deconvolution using only the spectrum of ***C***-, ***A***-, and ***X***-centers resulted in obvious poor-quality fits of the N-region due to absorption from ***Y***-centers. Consequently, a modified deconvolution routine was developed and integrated into a customized Excel spreadsheet (*Caxbd_Inherit_2024-Ib*, see Online Materials[1]) modified from the Caxbd_o2010 Excel spreadsheet (De Beers UK Ltd, Maidenhead 2010). This modified deconvolution routine allows one to account for absorption due to ***Y***-centers, in addition to ***C***-, ***A***-, and ***X***-centers, during deconvolution. The ***Y***-center reference spectrum used for deconvolution was taken from Hainschwang et al. (2012), where the N-region of ***Y***-center-rich *Type Ib* + *IaA* diamonds was decomposed by iteratively subtracting the spectrum of ***C***- and ***A***-centers until N_C and $N_A = 0$. The spectrum of ***Y***-centers (see Fig. 1) shows a broad absorption peak centered at ~1145 to 1150 cm^{-1}, a slightly weaker broad peak at 1261 to 1268 cm^{-1}, and sharper characteristic peaks at 1220 to 1240 cm^{-1} (Hainschwang et al. 2012). As the position of the main peak in the spectrum of ***C***- and ***Y***-centers is similar (1130 and 1145 cm^{-1}), least-squares fitting of a spectrum may converge to a false minimum if both the ***C***- and ***Y***-center components are unconstrained during refinement of the fit. Consequently, the ***C***-center component was manually constrained to the observed intensity of the characteristic peak at 1344 cm^{-1} (Dyer et al. 1965) as this peak is not observed in the ***Y***-center spectrum. Allowing the ***D***-component to refine freely during least-squares fitting resulted in a minimal ***D***-center component and negligible improvement to the fit. This is expected as ***D***-centers represent platelet (***B′***)-induced lattice absorption, and large platelets are only observed in *Type IaAB* and *IaB* diamonds (Clark and Davey 1984; Woods 1986). The ***X***-center component was manually constrained to the observed intensity of the peak at 1332 cm^{-1}. Although a peak at 1332 cm^{-1} is also observed for ***B***-centers, diamonds with significant ***C***- and ***B***-center content [e.g., ABC diamonds (Hainschwang et al. 2006)] are exceedingly rare, and no peak at 1172 cm^{-1} was observed in any of the spectra, and thus a null (or negligible) ***B***-center content was assumed for all spectra. Moreover, relatively weak broad peaks are observed at 1115 and 1046 cm^{-1} confirming the presence of ***X***-centers (Lawson et al. 1998).

For all spectra, N_C, N_A, and N_X [and $N_C(Y)$, $N_A(Y)$, and $N_X(Y)$ in at. ppm] were calculated using the following absorption coefficients [***C***-centers] = 25 at. ppm × μ1130 cm^{-1} (Chrenko et al. 1971; Kiflawi et al. 1994); [***A***-centers] = 16.5 at. ppm × μ1282 cm^{-1} (Boyd et al. 1994; Kiflawi et al. 1994); and [***X***-centers] = 5.5 at. ppm × μ1332 cm^{-1} (Lawson et al. 1998). ***C***-center contents calculated using the alternative absorption coefficient [***C***-centers] = 37 at. ppm × μ1344 cm^{-1} (Liggins 2010) were in good agreement (5–10%) with those calculated using [***C***-centers] = 25 at. ppm × μ1130 cm^{-1} (Chrenko et al. 1971; Kiflawi et al. 1994) except for some spectra with low N_{tot} (<30 at. ppm) that also showed poor signal-to-noise ratios and thus were not

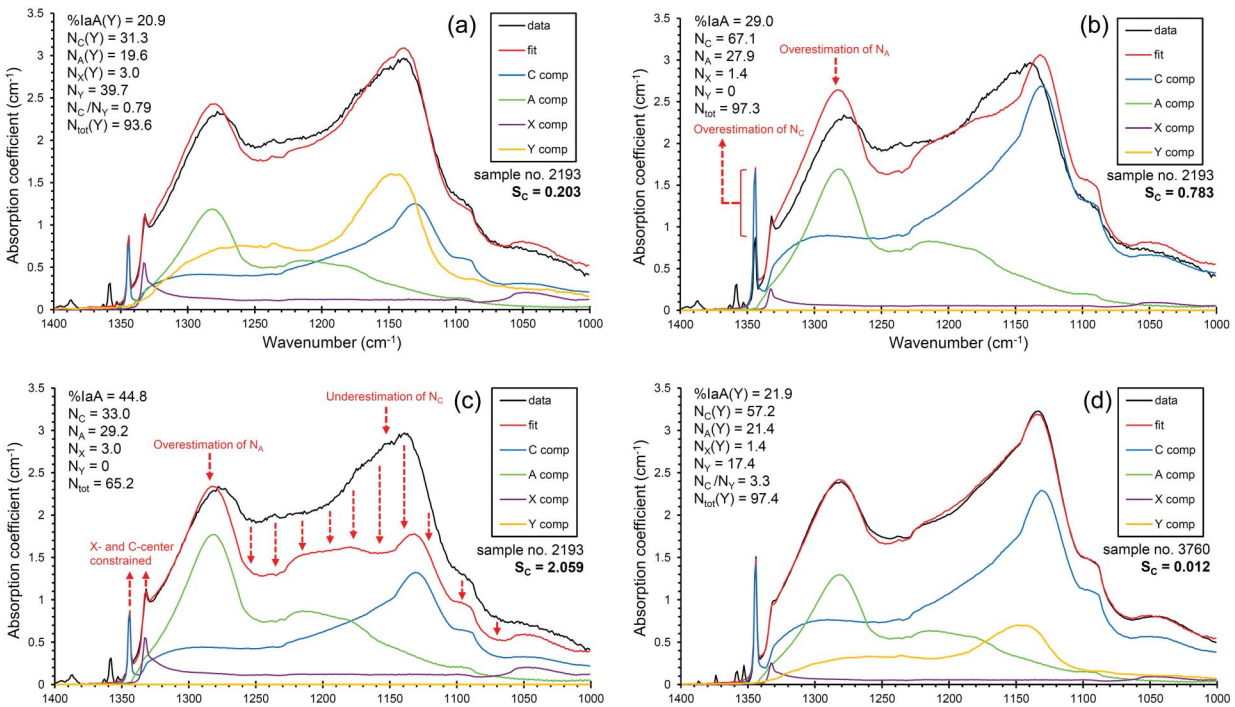


Figure 1. The least-squares fitting and deconvolution results of the N-region in the IR spectrum of (**a**) sample #2193, where ***Y***-centers were incorporated during deconvolution; (**b**) sample #2193, where ***Y***-centers were not incorporated during deconvolution and N_C, N_X, and N_A were freely refined; (**c**) sample #2193, where ***Y***-centers were not incorporated during deconvolution, N_C and N_X were constrained to the height of the 1344 and 1332 cm^{-1} peaks, respectively; and (**d**) sample #3760 where ***Y***-centers were incorporated during deconvolution. Note the higher quality fit (S_C) in (**a**) and (**d**) and how N_C and N_A are overestimated in (**b**) and how N_C is underestimated and N_A overestimated in (**c**). Refer to "Terminology and nomenclature" for explanations of all terms.

Downloaded from pubs.geoscienceworld.org/msa/ammin/article-pdf/111/3/360/7778962/ammin-2025-9722.1.pdf by guest on 30 October 2026

included. Although Hainschwang et al. (2012) recommend using the absorption coefficient [*C*-centers] = 37 at. ppm × μ1344 cm^{-1} when there is significant absorption due to *Y*-centers, the 1344 cm^{-1} peak in some spectra is too weak to be reliably fitted or differentiated from noise due to atmospheric H_2O. Here, the *C*-center component is constrained to the height of the 1344 cm^{-1} peak (where possible) during least-squares fitting, and the absorption coefficient [*C*-centers] = 25 at. ppm × μ1130 cm^{-1} is used to calculate N_C [and $N_C(Y)$]. Where the 1344 cm^{-1} peak is too weak or not observed, μ1130 cm^{-1} is not constrained during least-squares fitting. In some cases, the relative intensity of the 1344 cm^{-1} peak compared to that in the *C*-center reference spectrum may vary due to strain. Where this is the case, constraining the *C*-center component to the 1344 cm^{-1} peak intensity will not produce reliable *C*-center contents. Although this was apparent in only a handful of samples, it was easily recognized due to low-quality fits from 1150 to 1130 cm^{-1} and rectified by freely refining the *C*-center component. The relative intensity of the 1332 cm^{-1} peak may also vary with respect to that of the *X*-center reference spectrum due to changes in local symmetry and interaction with other defects (Liggins 2010). If one suspects this is the case, it is recommended that the *X*-center component be freely refined instead of constraining it to the observed intensity of the 1332 cm^{-1} peak.

The identity and absorption coefficient of the *Y*-center are unknown. However, several authors describe evidence showing that *Y*-centers are related to defects that contain single substitutional N (*C*- or *X*-centers) (e.g., Hainschwang et al. 2012; Titkov et al. 2015a, 2015b). The similar position of the *C*- and *Y*-center absorption maxima (1130 and 1145 cm^{-1}, respectively) may indicate a similar (IR-active) N-C bond as IR peak positions are sensitive to both bond strength (i.e, N-C bond energy) and the identity of each participating element (i.e., reduced mass of N and C). Moreover, we identify a discrete peak, located at 1358 cm^{-1}, that is positively correlated with *Y*-centers (Hainschwang et al. 2012; Reutsky et al. 2017), and may represent a local vibrational mode of the *Y*-center absorption system, similar to the 1344 cm^{-1} peak associated with *C*-centers. In this context, one can envision the *Y*-center absorption system as being shifted, with respect to the *C*-center absorption system, by ~15 cm^{-1} to higher frequencies (i.e., 1130 cm^{-1} shifted to 1145 cm^{-1} and 1344 cm^{-1} shifted to 1358 cm^{-1}).

For the reasons described above, we assign the absorption coefficient for *C*-centers to *Y*-centers ([*Y*-centers] = 25 at. ppm × μ1145–1150 cm^{-1}). The validity of this assignment was tested using two different methods (see Online Materials[1] Appendix A1), the results of which support this assumption, suggesting the *Y*-center absorption is between 19 and 41 at. ppm/cm^{-1}. This assumption allows calculation of the *Y*-center content (N_Y [at. ppm]) and thus $N_{tot}(Y)$ and the N-aggregation state: $\%IaA(Y) = 100 \times N_A(Y)/[N_A(Y) + N_C(Y) + N_X(Y) + N_Y)]$. Assigning the absorption coefficient of *C*-centers to *Y*-centers introduces some degree of uncertainty into the calculation of %IaA(Y) and $N_{tot}(Y)$. However, it produces more accurate (and precise) N-defect concentrations (higher-quality fits of the N-region) than the approach currently used in the literature, where absorption due to *Y*-centers is ignored and all intensity from 1150–1130 cm^{-1} is fitted with the spectrum of *C*-centers.

In Online Materials[1] Appendix A2, statistical methods used to assess fits of the N-region and the statistical significance of data correlations are described. Moreover, the bulk (averaged) nature of the FTIR spectra and its potential effect on the observed trends is discussed.

Results

Deconvolution of the N-region: The Effect of *Y*-Centers

The deconvolution results for selected spectra are shown in Figure 1, determined with (Figs. 1a and 1d) and without (Figs. 1b and 1c) incorporating *Y*-centers during fitting. Results for sample #2193 determined using the new deconvolution routine (with *Y*-centers incorporated) are shown in Figure 1a. Results determined without incorporating *Y*-centers and by freely refining N_C (μ1344 cm^{-1}) and N_X (μ1332 cm^{-1}) are reported in Figure 1b, where a much lower quality fit is obtained ($S_C = 0.783$) compared to the fit shown in Figure 1a ($S_C = 0.203$). Comparing Figures 1a and 1b shows that neglecting *Y*-centers during deconvolution of the FTIR spectrum of *Type Ib + IaA* diamonds may result in overestimation of μ1344 cm^{-1} (and thus N_C) and μ1282 cm^{-1} (and thus N_A; Fig. 1b) (Hainschwang et al. 2012). To correct for this overestimation, N_C (μ1344 cm^{-1}) and N_X (μ1332 cm^{-1}) are constrained to the observed intensity of the corresponding peaks (e.g., Fig. 1c) in previous studies. However, this also results in a poor-quality fit ($S_C = 2.059$) and underestimates N_{tot} (65.2 compared to 97.3 at. ppm) as all composite absorption due to *Y*-centers in not accounted for (Fig. 1c). To validate our new deconvolution results, we evaluate whether the signal associated with *Y*-centers is in fact due to a discrete defect, as opposed to an artifact associated with the *C*-center absorption system. As there is no positive correlation (proportionality) between μ1130 cm^{-1} and μ1145–1150 cm^{-1} (Online Materials[1] Fig. B1), *C*- and *Y*-centers must be discrete defects that may occur in variable proportions and form via different aggregation sequences. This is further demonstrated by comparing the spectra in Figures 1a and 1d, which have similar %IaA(Y) and $N_{tot}(Y)$ but significantly different $N_C(Y)$ and N_Y, i.e., $N_c(Y)/N_Y$ ratios of 3.3 and 0.79, respectively. In almost all spectra, evidence of *Y*-centers was observed, and significantly higher quality fits of the N-region were obtained when *Y*-centers were included during deconvolution. A comparison of the deconvolution results obtained using DiaMap (%IaA and N_{tot} determined without *Y*-centers) and our method [%IaA(Y) and $N_{tot}(Y)$ determined with *Y*-centers] is provided for selected spectra in Table 1 and for all spectra in Online Materials[1] Table C2. Additional peaks from ~1350 to 1390 cm^{-1} related to (self-)interstitial-related defects (Dischler 2012; Hainschwang et al. 2012) are observed in most spectra. The normalized intensities of such peaks are also reported for selected spectra in Table 1 and for some spectra in Online Materials[1] Table C2. A series of complete spectra from Online Materials[1] Table C2 is plotted in Online Materials[1] Figure B2 as a function of increasing %IaA(Y).

Values calculated using DiaMap (%IaA and N_{tot}) and our method [%IaA(Y) and $N_{tot}(Y)$] show a positive linear correlation (Figs. 2a and 2b). This correlation is expected as the same absorption coefficient is used for the calculation of N_C and N_Y, and *Y*-centers are treated as single-substitutional N: i.e., $\%IaA(Y) = 100 \times N_A(Y)/[N_A(Y) + N_C(Y) + N_X(Y) + N_Y]$. However, the effect of incorporating *Y*-centers is observed as increasing dispersion about the identity line as $N_{tot}(Y)$ increases (Fig. 2b). As shown in Figure 2c, there is good agreement between N_{tot} and $N_{tot}(Y)$ [$N_{tot} - N_{tot}(Y) \leq$ ~20 at. ppm] for samples with relatively low N_C, as either the majority of absorption in the N-region is assigned to *A*-centers or $N_{tot}(Y)$ is relatively low. However, as $N_C(Y)$ increases, this agreement becomes considerably worse as samples with high N_C may also have high N_Y, which is not accounted for during conventional deconvolution (e.g., using DiaMap). Inspection of Figure 2c shows that fitting the N-region of diamonds containing *Y*-centers using only *C*- and *A*-centers may result in overestimation of N_{tot} by up to ~100 at. ppm. The cause of this overestimation is apparent in Figure 1b, where both N_C (μ1344 cm^{-1}) and N_A (μ1282 cm^{-1}) are overestimated during least-squares fitting to compensate for the absence of a *Y*-center component. In general, the degree to which N_{tot} is overestimated increases with decreasing N_C/N_Y ratios. If N_C and N_X are constrained to the observed peak intensities of 1344 and 1332 cm^{-1} (e.g., Fig. 1c), N_A is drastically overestimated and N_{tot} is underestimated. The difference between %IaA and %IaA(Y) plotted as a function of $N_C(Y)$ (Fig. 2d) shows that incorporation of *Y*-centers during deconvolution shifts the calculated aggregation state by ~±10 %IaA.

Downloaded from pubs.geoscienceworld.org/msa/ammin/article-pdf/111/3/360/7778962/ammin-2025-9722.1.pdf by guest on 30 October 2026

Table 1. Selected data from FTIR spectra of *Type Ib + IaA* diamonds

Sample no.	%IaA(Y)	N_C(Y) at. ppm	N_A(Y) at. ppm	N_X(Y) at. ppm	N_Y at. ppm	N_{tot}(Y) at. ppm	%IaA	N_{tot} at. ppm	N_{tot}-N_{tot}(Y)	%IaA-%IaA(Y)	1353 cm^{-1}	1358 cm^{-1}	1363 cm^{-1}	1374 cm^{-1}	1387 cm^{-1}
501986	22.9	17.5	10.9	1.27	17.9	47.6	33.4	45.4	−2.2	10.5	0.032	0.200	0.001	0.007	0.027
888257	23.9	27.5	16.5	2.20	22.9	69.1	30.0	66.0	−3.1	6.1					
390746	22.8	14.8	9.7	1.01	17.2	42.7	29.4	39.2	−3.5	6.6	0.044	0.159	0.007	0.019	0.013
665540	16.3	67.5	23.2	1.64	49.8	142.1	21.6	129.7	−12.4	5.3	0.182	0.588	0	0.093	0.247
643299	26.5	5.0	7.3	0.66	14.6	27.6	36.4	27.2	−0.4	9.9	0.024	0.115	0	0	0.017
761265	71.1	7.0	74.8	1.99	21.4	105.2	76.0	104.7	−0.5	4.9	0.016	0.123	0.151	0.033	0.043
112167	18.0	105.0	38.0	4.40	63.9	211.2	24.2	198.0	−13.2	6.2	0.186	0.373	0.024	0.125	0.186
187552	33.5	32.5	40.3	3.03	44.7	120.5	37.6	118.5	−2.0	4.1	0.058	0.381	0.022	0.020	0.066
546866	26.0	26.3	19.8	2.59	27.3	75.9	33.9	73.4	−2.5	7.9	0.064	0.328	0.123	0.104	0.197
501987	22.9	18.8	10.9	1.38	16.7	47.7	29.0	45.5	−2.2	6.1					
866797	4.4	17.5	2.0	1.38	24.7	45.6	9.9	33.3	−12.3	5.5	0.065	0.339	0.022	0.027	0.185
943822	12.0	8.8	2.6	0.83	9.2	21.3	21.0	20.5	−0.8	9.0					
626035	84.8	20.0	213.0	1.47	16.8	251.3	87.2	249.2	−2.1	2.4	0.143	0.084	0.041	0.053	0
210997	34.3	30.9	46.2	4.57	53.3	135.0	40.9	129.0	−6.0	6.6	0.156	0.268	0.031	0.093	0.086
507406	48.8	17.4	66.7	3.34	49.4	136.9	57.2	134.3	−2.6	8.4	0.162	0.315	0.053	0.087	0.102
023290	7.8	13.8	2.5	0.83	14.6	31.7	15.7	31.0	−0.7	7.9					
359358	19.3	14.0	7.0	1.10	14.3	36.4	28.6	34.6	−1.8	9.3					

Notes: The concentration of ***C***-, ***A***-, ***X***-, and ***Y***-centers (N_C, N_A, N_X, and N_Y content, at. ppm), the total N content [N_{tot}(Y)], and the N-aggregation state [%IaA(Y)] were calculated by incorporating the ***Y***-center spectrum in the deconvolution routine using the *Caxbd_Inherit_2024-Ib* Excel spreadsheet (Online Materials[1]). For the purposes of comparison, N_{tot} and %IaA were calculated using the conventional deconvolution routine using the DiaMap Excel spreadsheet, in which the ***Y***-center spectrum is not incorporated during deconvolution.

The Relationship Between N-Aggregation State (%IaA) and *Y*-Centers

Inspection of Figure 3a shows a positive linear correlation between %***X***(Y) and %***Y*** ($R^2 = 0.87$, $r = 0.62$). As ***X***-centers, and likely ***Y***-centers, are related to single-substitutional N, one might expect a similar linear correlation between %***Y*** [or %***X***(Y)] and %IaA(Y). However, this is not the case as shown in Figure 3b. Here, %***Y*** first increases up to %IaA(Y) = ~20 (green zone, Fig. 3b), then shows an approximately flat trend between %IaA(Y) = 20–40 (yellow zone, Fig. 3b) and finally decreases from %IaA(Y) = 40–90 (red zone, Fig. 3b). The same trend is observed in Figure 3c, where %***X***(Y) is plotted as a function of %IaA(Y) showing that an increase in %***X***(Y) coincides with the initial onset of ***A***-center formation, then plateaus between %IaA(Y) = 20–40 and then decreases linearly from %IaA(Y) = 40–90. Similar trends are also observed for %***X***(Y) and %***Y*** plotted as a function of %***C***(Y) (Online Materials[1] Figs. B3 and B4). These trends show that the formation mechanism of ***Y***-centers (and ***X***-centers) becomes inactive at ~20% IaA(Y) and, instead of aggregation products, ***Y***- and ***X***-centers become aggregation reagents at ~35–40% IaA(Y) where they likely combine with different types of *V*/N- or (self-)interstitial-related defects to eventually form ***A***-centers. The effect of this transitional behavior of ***Y***- and ***X***-centers is observed in Figure 3d, where there is relatively more scatter in %***C***(Y) from %IaA(Y) = 20–40, and N_Y and N_X(Y) reach peak concentrations.

Peak Intensity Correlations: The 1353 to 1387 cm^{-1} Peaks and *Y*-Centers

Several peaks, observed between 1353 and 1387 cm^{-1}, are commonly accompanied by a significant ***Y***-center component and thus have been tentatively assigned to local vibrational modes of the ***Y***-center absorption system (Hainschwang et al. 2012; Titkov et al. 2015a; Reutsky et al. 2017) in addition to other defects such as platelets [i.e., (self-)interstitial complexes]. However, as an approximation of ***Y***-center content has not been previously attempted, these peaks have not been rigorously investigated until now. The normalized intensities of peaks at 1353, 1358, 1363, 1374, and 1387 cm^{-1} are reported in Online Materials[1] Table C2. Additional peaks observed at 1348 and 1368 cm^{-1} are often observed in samples with $N_{tot}(Y) > 150$ at. ppm but are relatively weak and were not considered here. The IR spectrum of a *Type Ib + IaA* (18.4%IaA) specimen is shown in Figure 4a, and peaks observed between 1353 and 1387 cm^{-1} are shown in Figure 4b.

The intensities of the 1358 and 1387 cm^{-1} peaks are positively correlated with %***Y*** (Figs. 5a and 5b) defining a positive correlation between the 1358 and 1387 cm^{-1} peak intensities (Fig. 5c). The correlation observed in Figure 5a is much stronger ($R^2 = 0.78$, $r = 0.88$) compared to that observed in Figure 5b ($R^2 = 0.32$, $r = 0.57$) and the 1358 cm^{-1} peak intensity (and thus the 1387 cm^{-1} peak intensity, Online Materials[1] Fig. B5) is negatively correlated with %IaA(Y) (Fig. 5d). The intensities of the 1353 and 1374 cm^{-1} peaks show a relatively strong positive correlation ($R^2 = 0.92$, $r = 0.96$) (Fig. 6a) and generally increase with increasing N_{tot}(Y) (e.g., Fig. 6b and Online Materials[1]

Downloaded from pubs.geoscienceworld.org/msa/ammin/article-pdf/111/3/360/7778962/ammin-2025-9722.1.pdf by guest on 30 October 2026

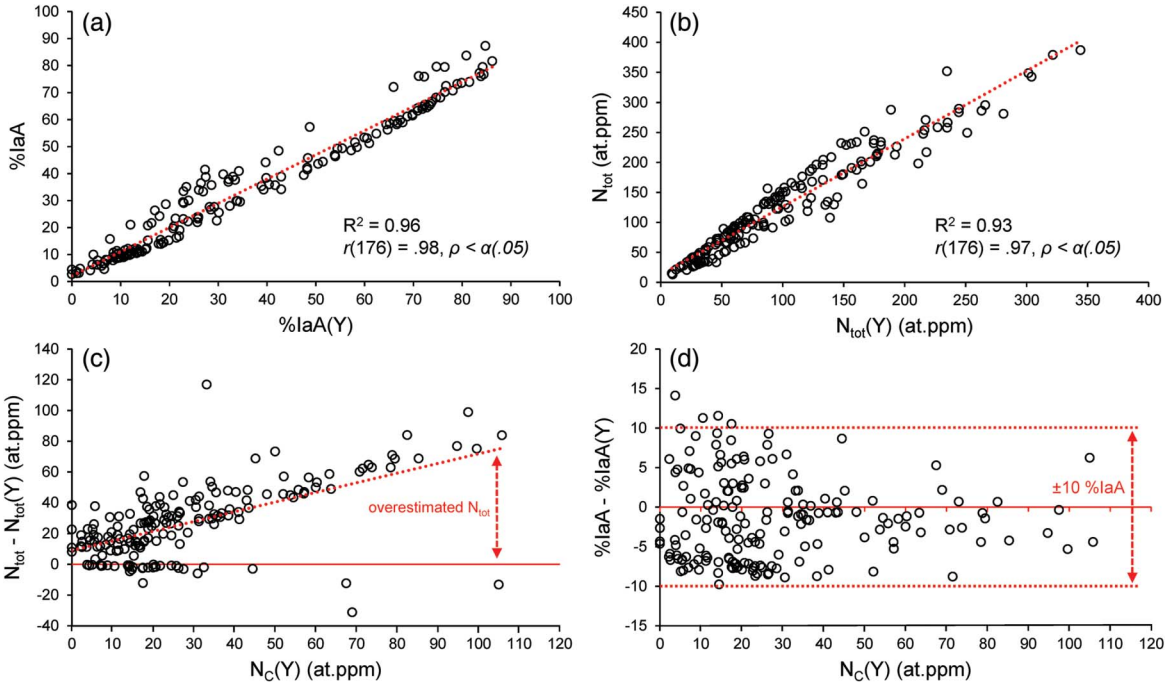


FIGURE 2. Comparison of (**a**) %IaA vs. %IaA(Y), (**b**) N_{tot} vs. $N_{tot}(Y)$, (**c**) N_{tot}-$N_{tot}(Y)$ vs. $N_C(Y)$, and (**d**) %IaA - %IaA(Y) vs. $N_C(Y)$. Note the effect of neglecting ***Y***-centers during deconvolution on N_{tot} (overestimation of >100 at. ppm) (**c**) and %IaA (variation of ± 10 %IaA) (**d**). Refer to "Terminology and nomenclature" for explanations of all terms.

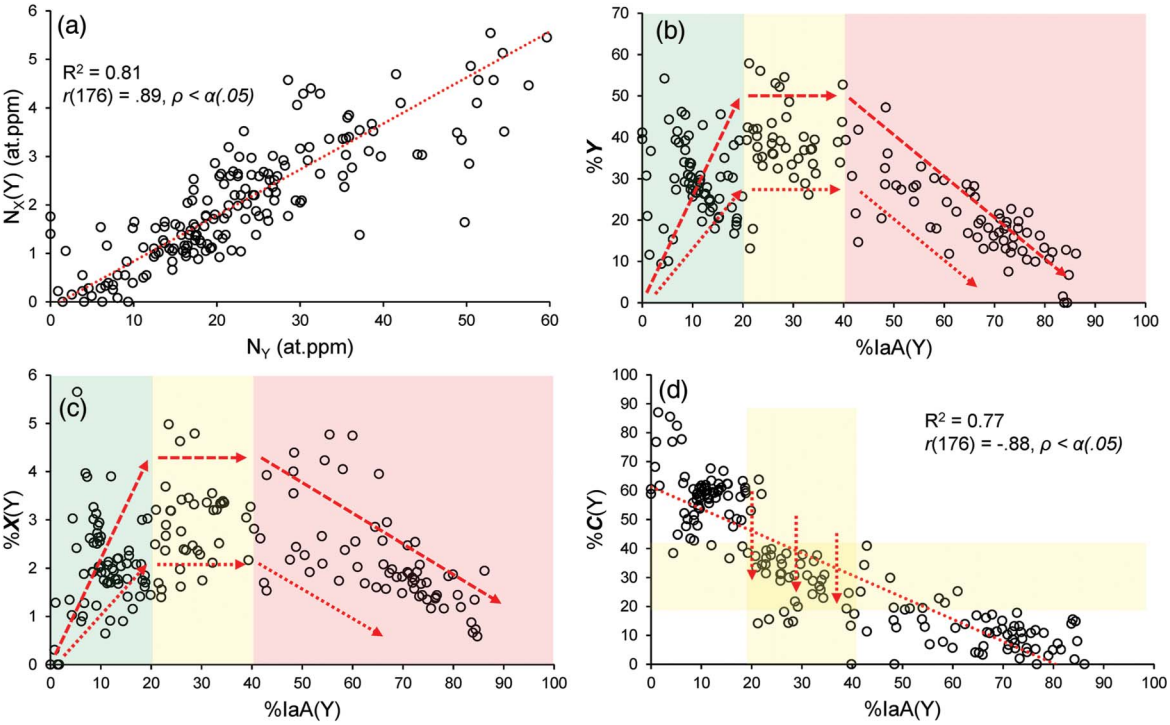


FIGURE 3. Comparisons of (**a**) $N_X(Y)$ vs. N_Y (at. ppm), (**b**) %***Y*** vs. %IaA(Y), (**c**) %***X***(Y) vs. %IaA(Y), and (**d**) %***C***(Y) vs. %IaA(Y). Note the trends in (**b**) and (**c**), which show that ***Y***-centers and ***X***-centers are intermediate defects that form between 0 and 40 %IaA(Y) and then are consumed between 40 and 100 %IaA(Y) to produce ***A***-centers. Maximum %***Y*** is observed between 20 and 40 %IaA(Y), this effect is observed as scatter between 20 and 40 %IaA(Y) in (**d**). Results of two-tailed *t*-tests are given in the format $r(df) = r$, ρα, where *df* is the degrees of freedom, *r* is the Pearson correlation coefficient, ρ is the ρ-value, and α is the significance level. Refer to "Terminology and nomenclature" for explanations of all terms.

Downloaded from pubs.geoscienceworld.org/msa/ammin/article-pdf/111/3/360/7778962/ammin-2025-9722.1.pdf by guest on 30 October 2026

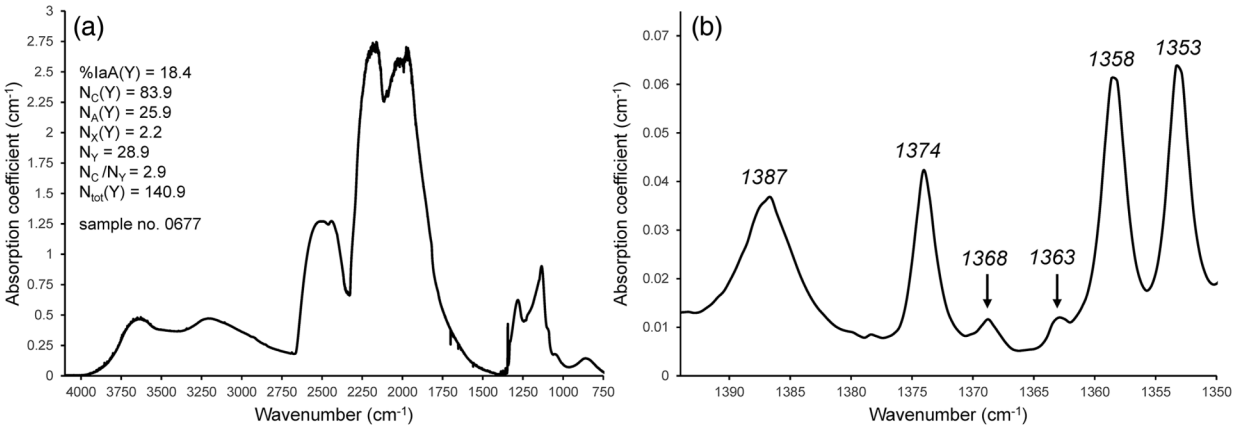


FIGURE 4. The IR spectrum of sample #0677 shown in the frequency range (**a**) 4100 to 750 cm^{-1} and (**b**) 1400 to 1350 cm^{-1} showing peaks at 1353, 1358, 1363, 1368, 1374, and 1387 cm^{-1} due to different types of (self-)interstitial complexes. This spectrum was baseline corrected and thickness normalized to the *Type II* reference spectrum used in the DiaMap Excel spreadsheet (Howell et al. 2012a, 2012b). Refer to "Terminology and nomenclature" for explanations of all terms.

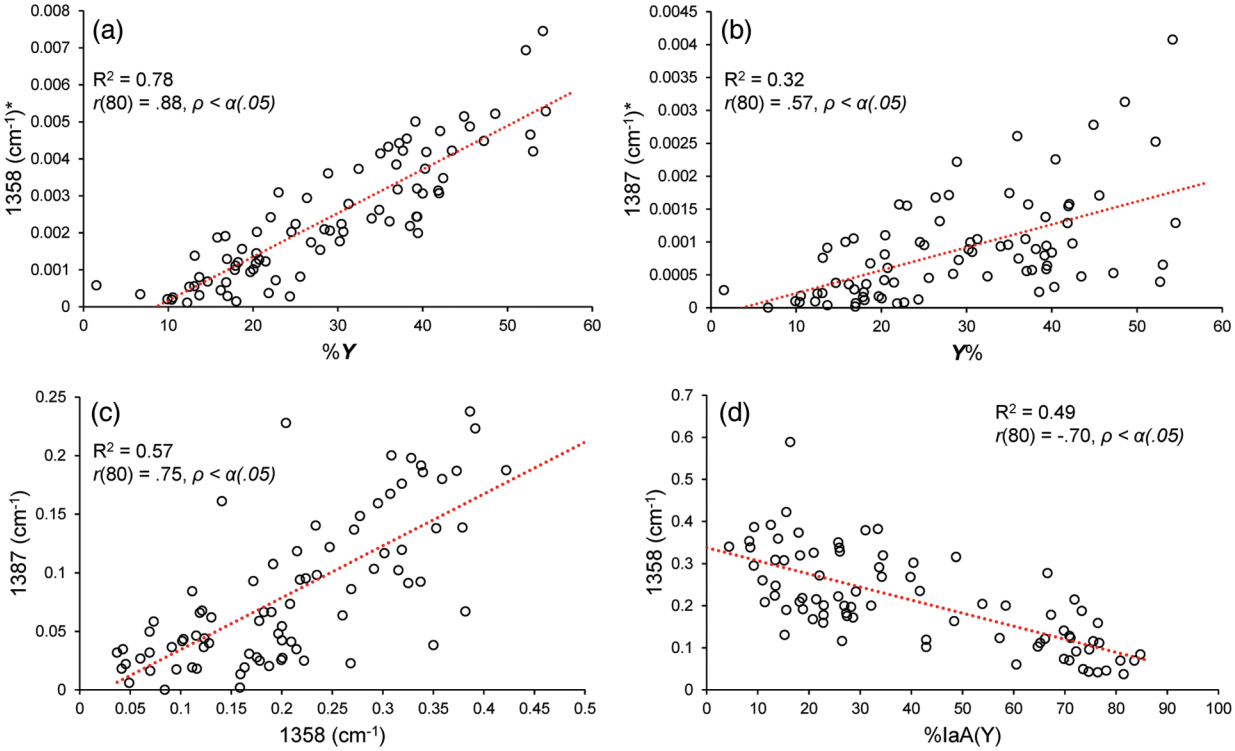


FIGURE 5. Comparisons of (**a**) the normalized 1358 cm^{-1} peak intensity and %***Y***, (**b**) the normalized 1387 cm^{-1} peak intensity and %***Y***, (**c**) the normalized 1387 and 1358 cm^{-1} peak intensities, and (**d**) the normalized 1358 cm^{-1} peak intensity and %IaA(Y). Note the strong positive linear correlation in (**a**) ($r = 0.88$, $R^2 = 0.78$) suggesting that the 1358 cm^{-1} peak may be a local vibrational mode of the ***Y***-center absorption system or that the (self-)interstitial complex that gives rise to the 1358 cm^{-1} peak is produced as a bi-product of ***Y***-center formation. The intensity of the 1358 and 1387 cm^{-1} peaks in (**a**) and (**b**) are normalized to N_{tot} [indicated as 1358 (cm^{-1})*] such that they can be compared to %***Y***. Results of two-tailed *t*-tests are given in the format $r(df) = r$, ρα, where *df* is the degrees of freedom, *r* is the Pearson correlation coefficient, ρ is the ρ-value, and α is the significance level. Refer to "Terminology and nomenclature" for explanations of all terms.

Fig. B6). However, no correlation is observed between the normalized 1353 cm^{-1} (or 1374 cm^{-1}, Online Materials[1] Figs. B7 and B8) peak intensity and N_Y or %IaA(Y) (Figs. 6c and 6d). The intensity of the 1363 cm^{-1} peak shows a weak positive correlation with %IaA(Y) ($R^2 = 0.31$, $r = 0.56$) (Fig. 7a) but no correlation with N_Y ($r = –0.02$) (Fig. 7b).

Downloaded from pubs.geoscienceworld.org/msa/ammin/article-pdf/111/3/360/7778962/ammin-2025-9722.1.pdf by guest on 30 October 2026

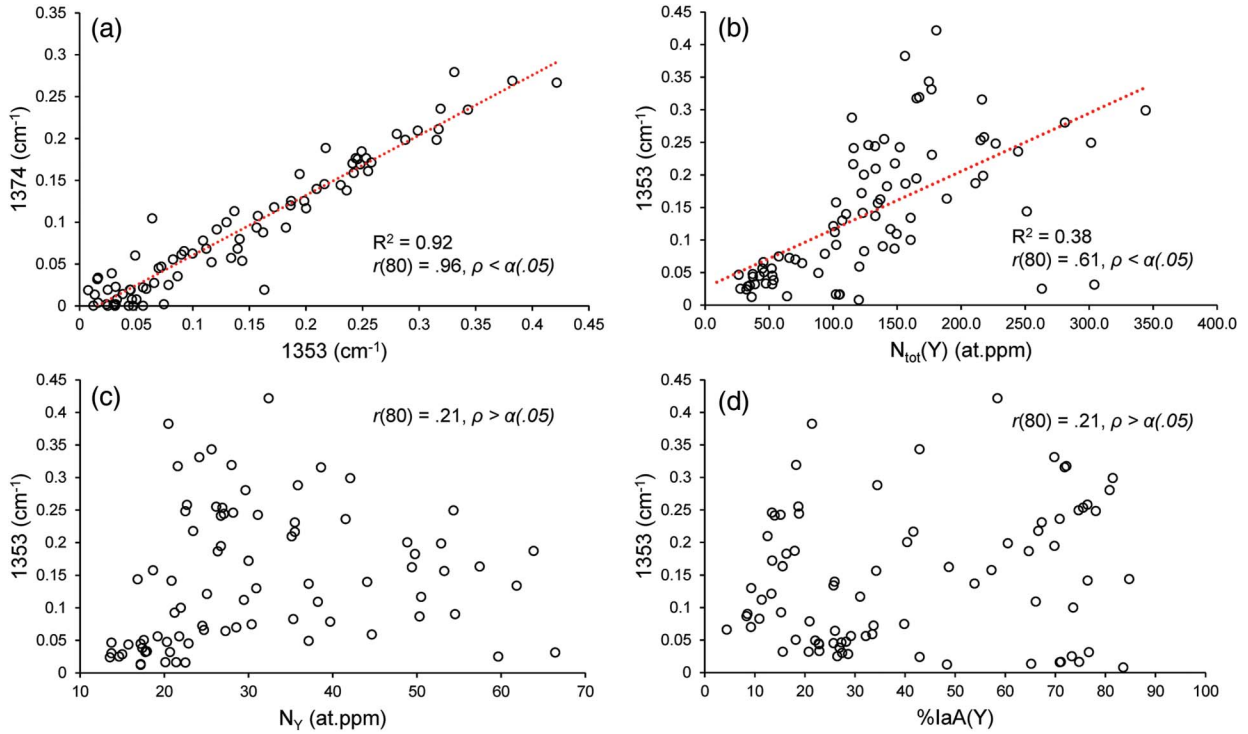


Figure 6. Comparisons of (**a**) the normalized 1374 and 1353 cm^{-1} peak intensities, (**b**) the normalized 1353 cm^{-1} peak intensity and $N_{tot}(Y)$, (**c**) the normalized 1353 cm^{-1} peak intensity and N_Y, and (**d**) the normalized 1353 cm^{-1} peak intensity and %IaA(Y). Note the strong positive correlation in (**a**), suggesting that the (self-)interstitial complexes that give rise to the 1374 and 1353 cm^{-1} peaks may be related to the same defect. Results of two-tailed *t*-tests are given in the format $r(df) = r$, ρα, where *df* is the degrees of freedom, *r* is the Pearson correlation coefficient, ρ is the ρ-value, and α is the significance level. Refer to "Terminology and nomenclature" for explanations of all terms.

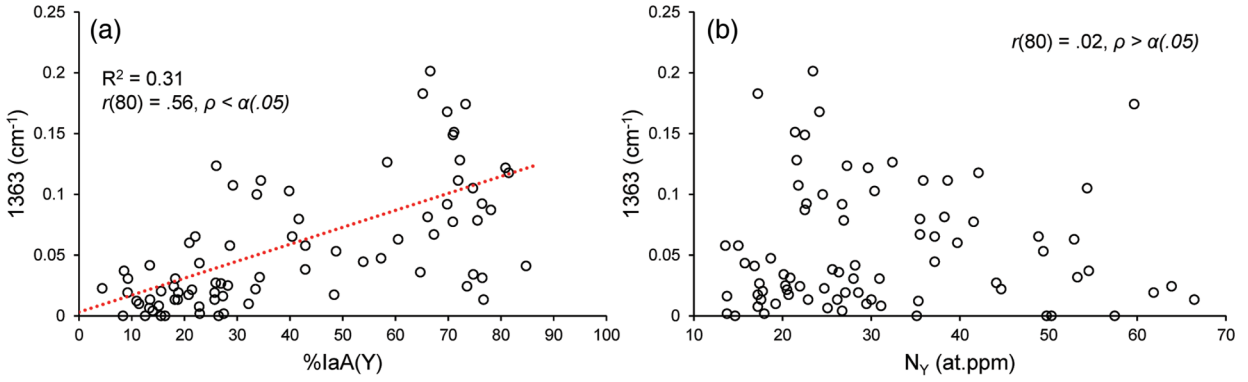


Figure 7. Comparisons of (**a**) the normalized 1363 cm^{-1} peak intensity and %IaA(Y), and (**b**) the normalized 1363 cm^{-1} peak intensity and N_Y. Results of two-tailed *t*-tests are given in the format $r(df) = r$, ρα, where *df* is the degrees of freedom, *r* is the Pearson correlation coefficient, ρ is the ρ-value, and α is the significance level. Refer to "Terminology and nomenclature" for explanations of all terms.

Discussion

Correcting Mantle Residence Time and Temperature Using *Y*-Centers

To demonstrate the effect of ***Y***-centers on calculated %IaA and N_{tot}, and thus mantle residence times/temperatures, we provide the following examples where we assume a ***C→A*** activation energy, $E_a = 5.5 \pm 0.7$ eV (Kiflawi et al. 1997), and that the rate of ***A***-center formation behaves according to second-order kinetics (Satoh et al. 1990; Mainwood 1994; Taylor et al. 1996). Although typically, two separate activation energies are used for octahedral and cuboid growth morphologies (Taylor et al. 1996), these values were determined from experiments on synthetic diamonds before the rate-enhancing effect of transition metal impurities (e.g., Ni and Co) was known (Kiflawi et al. 1997; Jones et al. 2015). Moreover, there is no experimental evidence from natural diamonds that indicates the ***C→A*** activation

Downloaded from pubs.geoscienceworld.org/msa/ammin/article-pdf/111/3/360/7778962/ammin-2025-9722.1.pdf by guest on 30 October 2026

energy in octahedral sectors is lower than that in cuboid sectors, and thus we use $E_a = 5.5 \pm 0.7$ eV (Kiflawi et al. 1997).

Consider sample #547284 (Online Materials[1] Table C2), here N_{tot} and %IaA (determined without incorporation of ***Y***-centers) are 71.8 and 51.2 at. ppm, respectively. After reprocessing while incorporating ***Y***-centers, N_{tot}(Y) and %IaA(Y) are 57.3 and 61.0 at. ppm, respectively. If we assume an average mantle residence temperature of 800 °C, the corrected N_{tot}(Y) and %IaA(Y) values correspond to a ~200 Myr increase in mantle residence time from ~200 to ~400 Myr (see red arrow in Fig. 8a). If we assume a mantle residence temperature of 775 °C, a ~750 Myr increase in mantle residence time (from ~875 to ~1625 Myr) is required. If we assume higher residence temperatures of 900 °C and 1000 °C, an ~1.12 Myr and ~16.5 Kyr increase in mantle residence time is required, respectively. As expected, the effect of this correction is not as pronounced for residence temperature, for example, if we assume the residence time for sample #547284 is 100 Myr, the corrected N_{tot}(Y) and %IaA(Y) values correspond to a ~13 °C increase in mantle residence temperature (see red arrows in Fig. 8b). Additional plots at higher mantle residence temperatures (900 °C) and shorter residence times (10 Myr) are provided in Online Materials[1] Figures B15 and B16.

For the data studied here, we report errors in mantle residence times of up to ~750 Myr, due to deconvolution without the incorporation of ***Y***-centers, assuming a residence temperature of 775 °C, which is sufficiently low to allow for partial preservation of ***C***-centers. Apart from accurately determining residence time and temperature, accurate N_{tot}(Y) values calculated from IR spectra are crucial when evaluating the reliability of alternative techniques (e.g., SIMS) commonly used to quantify N_{tot} in diamond (Hauri et al. 2002; Kaminsky et al. 2024).

Early Aggregation of N-Related Defects and the Formation of *Y*-Centers

As previously proposed, our results suggest that ***Y***-centers may form as an intermediate byproduct of ***C*→*A*** aggregation. In general, the transformation of ***C***-centers to ***A***-centers is driven by: (1) vacancy-assisted and/or (2) (self-)interstitial-assisted aggregation processes. The originally proposed mechanism by which ***C***-centers (N_S^0) directly substitute for an adjacent C atom requires significantly higher E_a than (1) and (2) (Goss et al. 2003, 2004) and has been largely ruled out based on several experimental observations (Jones et al. 2015). Vacancy-assisted ***C*→*A*** ($N_S^0 \rightarrow N_2^0$) aggregation is simply described in the following sequence (Collins 1980):

$$N_S^0\ (\textbf{\textit{C}}\text{-center}) + V^0 \rightarrow NV^0 \quad (1)$$

$$N_S^0 + NV^0 \rightarrow VN_2^0\ (\textbf{\textit{H3}}\text{-center}) \quad (1.1)$$

$$VN_2^0 \rightarrow N_2^0\ (\textbf{\textit{A}}\text{-center}) + V^0 \quad (1.2)$$

Here, N_S^0 may donate electrons to the band-gap, resulting in the production of N_S^+ (***X***-centers) and negatively charged defects such as V^- (***ND1***-center) (Davies et al. 1992), where V^0 (***GR1***-center) (Collins 1982) acts as the dominant electron acceptor (Lawson et al. 1998). Here, sequences (1) and (1.1) can be modified accordingly to produce NV^- and VN_2^- (NVN^-, ***H2***-center) (Hainschwang et al. 2006):

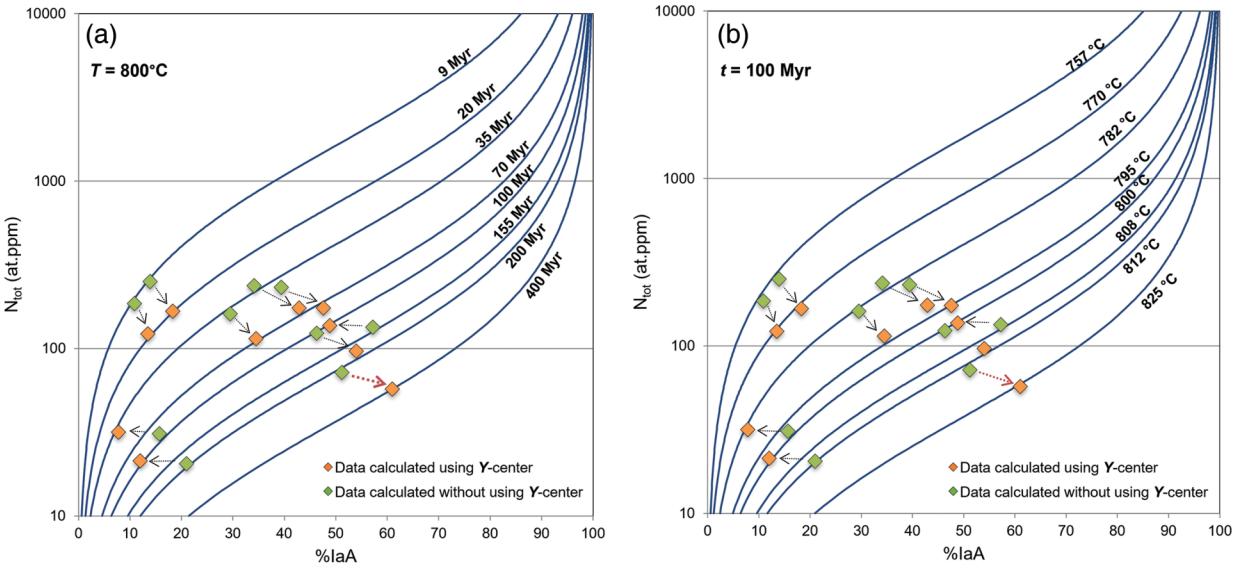


Figure 8. Total N content [N_{tot} (at. ppm)] plotted as a function of N-aggregation state (%IaA) where (**a**) 800 °C isotherms (blue lines) are plotted for residence times of 9 to 400 Myr and (**b**) 100 Myr isochrons are plotted for residence temperatures of 757 to 825 °C. To show the effect of ***Y***-centers on calculated mantle residence times or temperatures, N_{tot} and %IaA (green diamonds), determined without incorporation of ***Y***-centers, and N_{tot}(Y) and %IaA(Y) (orange diamonds), determined by incorporating ***Y***-centers, are plotted for selected samples. Arrows show the effect of correcting N_{tot} and %IaA [to N_{tot}(Y) and %IaA(Y)] on residence time and temperature. The red arrow represents sample #547284. Where %IaA is overestimated, there is minimal difference between N_{tot} and N_{tot}(Y) (see arrows pointing from right to left). Isotherms were calculated and plotted by modifying the second-order rate equation formula from DiaMap (Howell et al. 2012a, 2012b). The ***C*→*A*** activation energy, $E_a = 5.5$ eV, determined by Kiflawi et al. (1997), was used to calculate residence time/temperatures.

Downloaded from pubs.geoscienceworld.org/msa/ammin/article-pdf/111/3/360/7778962/ammin-2025-9722.1.pdf by guest on 30 October 2026

$$N_S^0 + V^- \rightarrow NV^- \quad (2)$$

$$N_S^0 + NV^- \rightarrow VN_2^- \ (\textbf{\textit{H2}}\text{-center}) \quad (2.1)$$

For sequences (1)–(2) to proceed, a mechanism by which V^0 and V^- are produced is required. In diamonds, V^0 and V^- are produced by different types of irradiation (Collins 1982) (from minerals and fluids or by man-made treatment) or by various deformation mechanisms, e.g., plastic deformation and the subsequent production of lattice dislocations (Hull and Bacon 1984; Fisher et al. 2009). For natural *Type Ib + IaA* diamonds from the Zimmi alluvial locality (West Africa), Smit et al. (2018) explain the production of V^0 and V^- and the preservation of ***C***-centers by exhumation-related deformation where shear-stress due to exhumation resulted in lattice dislocations [evidenced by a "band A" observed in cathodoluminescence (CL) spectra (Graham et al. 1991)] and the production of V^0 and V^-. The proposed exhumation to residence temperatures of 650–700 C° [significantly lower than average mantle residence temperatures of 1000 to 1100 C° (Stachel and Luth 2015)] drastically slowed the rate of ***C*→*A*** aggregation thus preserving N_S^0 while allowing for continued V^0, V^-, NV^0, and NV^- migration/aggregation which requires temperatures ≥600 C° (Dale 2015).

If one assumes that ***C*→*A*** aggregation is driven largely by a vacancy-assisted mechanism, it is tempting to assign NV and/or VN_2 (in the neutral or negative charge-state) to ***Y***-centers as both defects are produced as intermediates in sequences (1) and (2) (Collins 1980). Although evidence for such defects is frequently observed in UV-vis and PL spectra of natural *Type Ib + IaA* diamonds (e.g., Smit et al. 2018; Mashkovtsev et al. 2021), no rigorous correlations between the intensities of peaks attributed to NV^0 and VN_2^0 (or NV^- and VN_2^-) and ***Y***-centers have been reported. However, the absence of such a correlation does not necessarily preclude the involvement of ***Y***-centers with the production of these defects as VN_2^0 and VN_2^- can also form by ***A***-centers trapping V^0 or V^- (Kiflawi and Lang 1976; Van Enckevort and Visser 1990) or by disassociation of ***A***-centers and the subsequent formation of NV^0 and NV^- (Kiflawi and Bruley 2000). If one assumes ***X***-centers (N_S^+) serve as the primary electron donors in the diamonds studied here, it is unlikely that electron acceptors (negatively charged vacancy-related defects, e.g., NV^- and/or VN_2^-) occur at significant concentrations, as they must occur in equilibrium concentration with N_S^+ [average $N_X(Y) = 2.2$ at. ppm].

Alternatively, the positive correlation observed between $N_X(Y)$ and N_Y (Fig. 3a) and the similar behavior of %***X*** and %***Y*** with increasing %IaA(Y) (Figs. 3b and 3c) may lead one to assume ***Y***-centers represent some variant of ***X***-centers (N_S^+) or are produced by similar charge-transfer processes. Titkov et al. (2015a) observed two EPR centers [M5- and M6-centers (Mineeva et al. 2013)] associated with ***C***-centers (denoted as ***P1***-center in EPR spectra) and suggest they may be due to N_S^0 in an excited state where electrons of N_S^0 couple with distant N_S^+ (separated by 8–10 interatomic spacings). Titkov et al. (2015a) suggest this type of extended defect may be responsible for ***Y***-center absorption. However, if this were the case, one must assume coupling of N_S^0 and N_S^+ does not shift the 1332 cm^{-1} peak. Furthermore, this type of extended defect does not explain the correlations observed between 1358 cm^{-1} (and 1387 cm^{-1}) and %***Y*** unless one assumes these peaks are derivatives of the 1332 cm^{-1} (N_S^+) and 1344 cm^{-1} (N_S^0) peaks that are frequency-shifted due to coupling (electronic interaction) between N_S^0 and N_S^+. However, if this was the case, and the formation of ***Y***-centers shifts the 1332 and 1344 cm^{-1} peaks to higher wavenumbers, one would expect a negative correlation between $N_X(Y)$ and N_Y (i.e., as more ***Y***-centers form, an increasing proportion of absorbance at 1332 cm^{-1} is shifted), but this is not the case as shown in Figure 3a. Based on our data, it is more likely that the linear trend in Figure 3a is, at least in part, a reflection of increasing $N_{tot}(Y)$ as both %***X***(Y) and %***Y*** decrease similarly with increasing $N_{tot}(Y)$ (see Online Materials[1] Figs. B9 and B10). Alternatively, the positive correlation observed in Figure 3a may suggest that the formation of ***Y***-centers may be due to electron charge transfer with ***X***-centers (N_S^+). However, more work on other defects common in *Type Ib* diamonds that may accept electrons from N_S^+ (e.g., NV^- and VN_2^-) (Luo and Breeding 2013; Fritsch and Delaunay 2018; Smit et al. 2018; Kazuchits et al. 2021) is required. Moreover, the existence of diamonds that contain almost exclusively ***Y***- or ***X***-centers (e.g., Hainschwang 2014; Reutsky et al. 2017) suggests that the formation of ***Y***-centers is not solely reliant on charge transfer from ***X***-centers.

Evidence of (Self-)Interstitial-Assisted Aggregation

Above, vacancy-assisted aggregation is discussed as a mechanism for the formation of ***Y***- and ***A***-centers. Next, attention is turned to alternative aggregation mechanisms involving (self-) interstitial atoms and the complexes they form. Peaks at 1353, 1358, 1363, 1374, and 1387 cm^{-1} are observed in most spectra studied here. In *Type IaAB* and *IaB* diamonds, some similar peaks are commonly attributed to platelets of varying size (nano- to micrometers in size) and composition (C_i, N_i, and V contents) (Woods 1986; Dischler 2012; Speich et al. 2017). However, such platelets are thought to form as a byproduct of ***A*→*B*** aggregation and the subsequent generation and accumulation of C_i (via $N_2 + N_2 = VN_4 + C_i$). In natural *Type Ib* diamonds, the formation of vacancies, and thus interstitials, relies partly on deformation- and irradiation-related mechanisms (Smit et al. 2018). However, low mantle resindence times (t)/temperatures (T) and potentially low interstitial content limit the accumulation of interstitials, and instead, small (usually 1–4 atoms) (self-)interstitial complexes form (Goss et al. 2003, 2004). This series of peaks is common in *Type Ib* diamonds and is often associated with interstitials or platelets (e.g., Lai 2018; Lai et al. 2020b, 2024; Vasilev et al. 2024).

Based on theoretical work (Goss et al. 2004), upon irradiation of *Type Ib* diamond, C_i is trapped by N_S^0 to form (N_S^0-C_i), with progressive annealing, this complex disassociates, releasing mobile C_i and N_i, which in-turn, may recombine with (N_S^0-C_i) and N_S^0 to form (N_i-C_i) and (N_S^0-N_i) complexes. The formation of (N_S^0-N_i) and its eventual reconfiguration to (N_2-C_i) (Goss et al. 2004) can be generally described as:

$$N_S^0 + C_i \rightarrow (N_S^0\text{-}C_i) \quad (3)$$

$$(N_S^0 + C_i) + N_i \rightarrow (N_S^0\text{-}N_i) + C_i \rightarrow (N_2\text{-}C_i) \quad (3.1)$$

$$(N_2\text{-}C_i) + \text{annealing } T/t \rightarrow N_2^0\ (\textbf{\textit{A}}\text{-center}) + C_i \quad (3.2)$$

Here, (N_2-C_i) forms when N_i combines with N_S^0 where both N atoms substitute for a single C atom that is subsequently trapped

Downloaded from pubs.geoscienceworld.org/msa/ammin/article-pdf/111/3/360/7778962/ammin-2025-9722.1.pdf by guest on 30 October 2026

as an interstitial (C_i) (Liggins 2010). At sufficient annealing temperatures, (N_2-C_i) disassociate to form ***A***-centers (N_2^0) by releasing C_i (Nadolinny et al. 2000; Goss et al. 2004; Jones et al. 2015), an example of how (self-)interstitials drive ***C→A*** aggregation. Here, (N_2-C_i) is often referred to as the ***H1a***-center. However, several energetically reasonable structural models have been proposed for the ***H1a***-center, and a general consensus on a structural configuration for this defect has not been reached. In sequence (3.2), the release of C_i is important as it promotes the continued production of different N_i, (N_i-C_i)-related interstitial complexes and (N_2-C_i), that when annealed, will eventually form ***A***-centers (Kiflawi et al. 1997; Nadolinny et al. 2000). In turn, N_i- and (N_i-C_i)-related interstitial complexes continue to drive aggregation by combination with N_S^0 (Goss et al. 2004). Two examples of these alternative intermediate sequences are described as follows:

$$N_S^0 + C_i \rightarrow N_i \tag{4}$$

$$N_i + N_S^0 \rightarrow (N_2\text{-}C_i) + \text{annealing } T/t \rightarrow N_2^0 + C_i \tag{4.1}$$

$$N_S^0 + (C_i)_2 \rightarrow (N_i\text{-}C_i) \tag{5}$$

$$(N_i\text{-}C_i) + N_S^0 \rightarrow (N_i\text{-}N_i) \tag{5.1}$$

$$(N_i\text{-}N_i) + V \rightarrow N_i + N_S^0 \rightarrow (N_2\text{-}C_i) + \text{annealing } T/t \rightarrow N_2^0 + C_i \tag{5.2}$$

Sequences (3)–(5) assume that there is an active mechanism by which interstitials (C_i and N_i) are generated in sufficient concentrations. As is the case with *V*, irradiation and/or temperature- and pressure-induced plastic deformation, causing the formation of dislocations, may generate interstitials (Collins 1982; Smit et al. 2018). Moreover, the presence of transition-metal impurities (e.g., Ni), that readily substitute for C, producing C_i (Nadolinny et al. 2000; Jones et al. 2015), may also drive initial transformation of ***C***-centers to ***A***-centers via (self-)interstitial-assisted aggregation sequences. Evidence of plastic deformation is present in the diamonds studied here, in the form of amber centers (Massi et al. 2005; Hainschwang et al. 2020), which are observed as broad bands at 4064 and 4109 cm^{-1}. However, no correlation between the intensity of such bands and any peaks in the one-phonon region was observed.

Of the peaks listed above, the 1358 cm^{-1} peak shows the strongest positive correlation with %***Y*** (Fig. 5a) and a relatively weaker correlation with %***X***(Y) (see Online Materials[1] Fig. B11). This observation is in agreement with the findings of Reutsky et al. (2017) who observed a correlation between the 1332 and 1358 cm^{-1} peaks. Consequently, this peak may represent a local vibrational mode of the ***Y***-center absorption system (Hainschwang et al. 2012), akin to the sharp peaks at 1344 and 1332 cm^{-1} associated with the ***A***- and ***X***-center absorption systems, respectively. It is tempting to assign the 1358 cm^{-1} peak to the intermediate (N_2-C_i) defect. However, the ***H1a***-center produces a characteristic IR peak at ~1450 cm^{-1} (Liggins et al. 2010) which is not observed in any of the spectra studied here suggesting that the formation of ***Y***-centers may inhibit formation of (N_2-C_i) and that (self-)interstitial-assisted ***C→A*** aggregation may proceed according to sequences different from (3.1)–(3.2), (4.1), and/or (5.2). The association of the ***Y***-center with any of the other complexes containing one or two N_i (and C_i) atoms is also problematic, as theoretical works suggest that such defects have local vibrational modes at much higher frequencies (1400–1900 cm^{-1}) (Goss et al. 2004; Salustro et al. 2018). Peaks in this region have been observed in natural *Type Ib + IaA* diamonds (e.g., Lai et al. 2020b) but are not observed here, likely due to noise from atmospheric H_2O. Alternatively, the 1358 cm^{-1} peak (and thus ***Y***-centers) may represent a slightly larger interstitial complex that is produced by the combination of smaller interstitial defects such as (N_S^0-N_i) or (N_S^0-C_i). Humble (1982) was the first to suggest that particular interstitial complexes serve as the building blocks for platelets, specifically the I_4 (tetra interstitial) complex composed of four C_i atoms. Several local vibrational modes of the I_4 complex 1349, 1362, and 1401 cm^{-1} (Goss et al. 2003) are close to peaks observed at 1353, 1358, 1363, 1374, and 1387 cm^{-1} as described above. Moreover, N_i, may replace C_i in the I_4 complex and other structural variants (e.g., the I_3 complex) producing potentially numerous vibrational modes in this region. Therefore, it is likely that some of the peaks in the 1350–1390 cm^{-1} region observed here are due to similar (self-) interstitial complexes. As the 1358 and 1387 cm^{-1} peaks are positively correlated with %***Y***, it is likely the ***Y***-center is associated with an interstitial complex that forms from ~0–40 %IaA(Y) (Fig. 3b). The intensity of the 1358 cm^{-1} peak decreases with increasing %IaA(Y) suggesting that this interstitial complex is eventually consumed to produce ***A***-centers. Based on the correlation observed in Figure 5c, similar interpretations about the 1387 cm^{-1} peak can be made. However, the correlation between the 1387 cm^{-1} peak intensity and %***Y***, as shown in Figure 5b, is much weaker than that observed in Figure 5a suggesting that the defect corresponding to the 1387 cm^{-1} peak may be involved in additional aggregation sequences distinct from those responsible for the formation of ***Y***-centers. As described above, platelet peaks are attributed to vibrational modes involving C_i and N_i in platelets (Clark and Davey 1984; Fritsch et al. 1991; Zaitsev 2001), and the intensity of such peaks is proportional to the signal attributed to ***D***-centers in *Type IaAB* and *IaB* diamonds (Woods 1986). Consequently, the ***D***-center has been attributed to platelet-stimulated lattice vibrational modes. If, in fact, ***Y***-centers are related to a (self-)interstitial complex, absorption in the lower-frequency N-region may also represent lattice perturbations associated with the N_i/C_i-related (self-)interstitial defect, akin to the ***D***-center in *Type IaA + IaB* diamonds.

As first observed by Fisher and Lawson (1998), there is strong positive correlation between the intensity of the 1353 and 1374 cm^{-1} peaks (Fig. 6a). Moreover, the 1353 and 1374 cm^{-1} peak intensity increases with increasing N_{tot}(Y) (Fig. 6b), unlike the 1358, 1363, and 1387 cm^{-1} peaks (see Online Materials[1] Figs. B12–B14), suggesting the 1353 and 1374 cm^{-1} peaks represent the same defect. The 1353 and 1374 cm^{-1} peak intensities do not show any correlation with N_Y (Fig. 6c) or %IaA(Y) (Fig. 6d), suggesting that the corresponding defects are not directly related to the formation of ***A***- or ***Y***-centers. The intensity of the 1363 cm^{-1} peak is positively correlated with %IaA(Y) (Fig. 7a) but shows no correlation with N_Y (Fig. 7b), suggesting that production of the corresponding defect is coupled with the formation of ***A***-centers (or consumption of ***C***-centers). In Figure 9, general trends in the ***C***-, ***Y***-, and

Downloaded from pubs.geoscienceworld.org/msa/ammin/article-pdf/111/3/360/7778962/ammin-2025-9722.1.pdf by guest on 30 October 2026

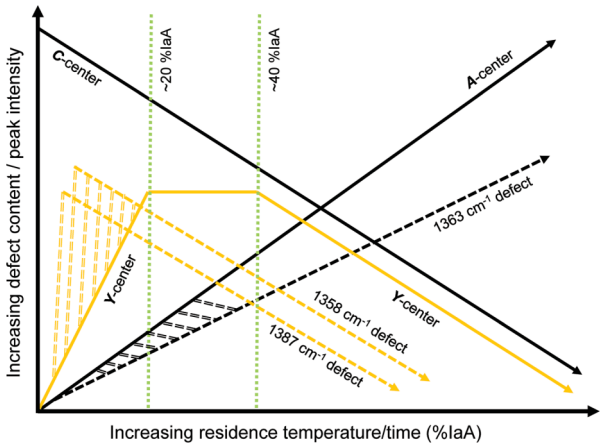


Figure 9. Illustration showing trends in defect content plotted as a function of %IaA(Y) (increasing mantle residence temperature/time). Solid black lines represent traditional ***C→A*** aggregation sequences. The 1363 cm^{-1} peak intensity increases with %IaA(Y) (dashed black line), and the corresponding defect is likely a byproduct of the formation of ***A***-centers (and the destruction of ***C***-centers) but is not correlated with ***Y***-center content. It follows that the 1363 cm^{-1} defect may form across a range of %IaA(Y) shown with the double dashed black lines. The 1353 and 1374 cm^{-1} peak intensities show no correlation with %IaA(Y) or ***Y***-center content and are therefore not plotted here. ***Y***-center content (solid yellow line) increases from 0–20 %IaA(Y), where additional defects that correspond to the 1358 and 1387 cm^{-1} peaks (yellow dashed lines) may be produced as byproducts of ***Y***-center formation. It follows that the 1358 and 1387 cm^{-1} defects may form from 0–20 %IaA(Y) (double dashed yellow lines). From 40–100 %IaA(Y) (solid yellow line), ***Y***-centers are consumed to produce ***A***-centers along with related defects that correspond to the 1358 and 1387 cm^{-1} peaks. It is also possible that the 1358 and 1387 cm^{-1} peaks represent vibrational modes of the ***Y***-center itself rather than discrete defects. Defect contents (*y*-axis) are not based on real data and instead are used to simply show variations in ***C***-, ***Y***-, and ***A***-center content (or peak intensities) as a function of %IaA(Y).

A-center content and different peak intensities are plotted as a function of %IaA(Y). Based on the trends described above and those shown in Figure 9, it is apparent that several different (self-)interstitial-assisted aggregation sequences may be operative during ***C→A*** aggregation. Interestingly, some diamonds contain almost exclusively ***X***- or ***Y***-centers, called *Type IbX* and *IbY* diamonds (Hainschwang 2014) in which no apparent ***C→A*** aggregation has occurred. Although such diamonds are not observed in this data set, such diamonds likely represent an unaggregated diamond in which the majority of ***C***-centers couple with (self-)interstitial complexes.

Untreated and Treated Natural *Type Ib* Diamonds

Thus far, ***Y***-centers have never been observed in synthetic diamonds. However, peaks attributed to platelets at similar positions (~1350–1375 cm^{-1}) have been produced via HPHT treatment of natural *Type Ib* + *IaA* yellow diamonds (Lai et al. 2020a) and synthetic diamond (Fisher and Lawson 1998). The ***H1a***-center (1450 cm^{-1} peak) has been produced by HPHT treatment of synthetic diamond, where its distribution in such diamonds suggests it is involved in ***C→A*** aggregation (Babich et al. 2016a, 2016b). These findings suggest HPHT-induced plastic deformation (in both synthetic and natural *Type Ib* diamond) may produce interstitials, which in turn, drive ***C→A*** aggregation via (self-)interstitial-assisted aggregation.

The behavior of ***Y***-centers during HPHT- and/or irradiation treatment is apparently much different from that observed for natural mantle annealing, as described here. In one study, HPHT treatment of natural *Type Ib* + *IaA* diamonds (at >2000 °C) resulted in a decrease in ***Y***-center absorption and the production of an unidentified peak at 1060 cm^{-1}; some production of ***A***-centers was also observed (Kupriyanov et al. 2020). In a different study, HPHT treatment of *Type IbY* diamonds resulted in disassociation of the ***Y***-center and subsequent production of ***C***-centers, a 480 nm band, and a 690 nm red luminescence band, but no production of ***A***-centers (Hainschwang 2014). Theoretical calculations indicate the 480 nm band may represent substitutional oxygen in the positive charge state (O^+) (Gali et al. 2001). An increase in the CO_2 peak intensity after HPHT treatment of some *Type IbY* diamonds has led to the assumption that O associated with ***Y***-centers is released upon heating and combines with C-O bonds to produce structurally bound CO_2 (Hainschwang et al. 2008). However, O contents have not been determined in diamonds with the 480 nm band (Lai et al. 2024), and no direct correlation has been found between ***Y***-centers and an O-related vibrational mode. Moreover, a recent study (Lai et al. 2024) shows that diamonds with the 480 nm band often contain several different Ni-related defects.

Hainschwang (2014) describes that HPHT-treatment of *Type IbY* diamonds results in a loss of ***Y***-centers that is not associated with the progressive formation of ***A***-centers, in stark contrast from what is discussed here (e.g., Fig. 3b). However, such HPHT-treatments were conducted at temperatures (typically 1700 to 2200 °C) and pressures (typically >6.5 GPa) that far exceed the estimated mantle residence conditions of *Type Ib* diamonds <800 °C (Smit et al. 2018, 2019) and even the conditions of natural diamond formation [1160 ± 100 °C and 5–6 GPa (Stachel and Harris 2009; Stachel and Luth 2015)]. It follows that the drastically different behaviors of ***Y***-centers observed during HPHT treatment and natural mantle annealing may reflect the instability of ***Y***-centers when subjected to extreme temperatures. Moreover, several different (dis)aggregation sequences become active at typical HPHT temperatures compared to normal mantle residence temperatures (e.g., Ashfold et al. 2020) and proceed at rates dependent on pressure and temperature, e.g., increasing pressure slows the rate of ***C→A*** aggregation (Kiflawi et al. 1997). Moreover, HPHT treatments are conducted on extremely short timescales (minutes to hours) compared to mantle residence times for *Type Ib* diamonds (tens to hundreds of millions of years). Although ***C→A*** aggregation is often induced during HPHT treatment (Chrenko et al. 1977), complex vacancy- or (self-)interstitial-assisted aggregation (that are active at only specific temperature ranges) may require annealing for significantly longer times than what is possible during HPHT treatment.

Implications

Based on the results of this study, in addition to numerous others completed over the last decade, it has become clear that ***Y***-centers represent a fundamental absorption system in most

Downloaded from pubs.geoscienceworld.org/msa/ammin/article-pdf/111/3/360/7778962/ammin-2025-9722.1.pdf by guest on 30 October 2026

natural *Type Ib + IaA* diamonds. As the exact identity and IR absorptivity of the ***Y***-centers remain unknown, the signal associated with this defect is commonly neglected during routine deconvolution (fitting) of the one-phonon region of *Type Ib + IaA* spectra. Using a new routine that incorporates the spectrum of ***Y***-centers during deconvolution, we demonstrate that fitting all aggregated intensity in the 1130–1150 cm^{-1} region with the spectrum of only ***C***-centers (and not ***Y***-centers) can result in an overestimation of N_{tot} by more than 100 at. ppm and variations in the N-aggregation state of ~±10 %IaA. These errors were determined for a sample set with an average N_{tot} of ~100 at. ppm and could be much larger for samples with higher N_{tot}. These errors translate to potentially large variations in calculated mantle residence times/temperatures (hundreds of Myr) and may lead to erroneous interpretations about the *P*/*T* (geologic) history of *Type Ib + IaA* diamonds and/or misleading interpretations based on agreement (or the lack thereof) with thermobarometric data obtained from mineral inclusions in diamond.

Our data suggest that ***Y***-centers are related to the (self-)interstitial-assisted aggregation of ***C***-centers and are likely composed of a (self-)interstitial complex involving N_S^0. Comparison of %***Y*** with %IaA(Y) shows that ***Y***-centers are an intermediate by-product of ***C***-to-***A*** aggregation produced when %IaA(Y) = 0–40, and then are consumed to produce ***A***-centers where %IaA(Y) = 40–100. Our results suggest IR peaks at 1353, 1358, 1363, 1374, and 1387 cm^{-1} may be due to (self-)interstitial complexes involving C_i and N_i atoms. A positive correlation between the normalized intensity of the 1358 and 1387 cm^{-1} peaks and %***Y*** suggests that ***Y***-centers may involve a (self-)interstitial point-defect (complex) involving both N_i/C_i and N_S^0. It follows that the 1358 and 1387 cm^{-1} peaks may represent local vibrational modes of the ***Y***-center. The intensity of the 1358 cm^{-1} peak decreases with increasing %IaA(Y) providing further evidence that (self-)interstitials serve as an important reagent in the transformation of ***C***-centers to ***A***-centers. Interestingly, in one study, upon HPHT treatment, ***Y***-centers disassociate to produce ***C***-centers and a 480 nm band, which has been attributed to substitutional O^+ (or Ni); however, no ***A***-centers are produced. Although this behavior is markedly different than what is observed here, temperatures, pressures, and annealing times associated with HPHT treatment are drastically different from those of the mantle residence environment of natural diamonds.

Although aggregation sequences involving interstitials generally have lower E_a compared to vacancy-related sequences (Kiflawi et al. 1996; Jones et al. 2015), it is possible that vacancy-assisted aggregation dominates in diamond where the vacancy content is significantly larger than the C_i and N_i content. Moreover, (self-)interstitial-driven aggregation does not preclude the involvement of vacancies, and it has been shown that vacancies may expedite (self-)interstitial-assisted aggregation [e.g., sequence (5.2)], and thus a combination of vacancy- and (self-)interstitial-assisted aggregation (e.g., Dale 2015) is likely operative in most *Type Ib + IaA* diamonds. This is evidenced by several *V*-related defects, such as NV^0 and VN_2^0 (or NV^- and VN_2^-), that are commonly observed in the UV and PL spectra of natural *Type Ib* diamonds and have been shown to form as intermediates during ***C*→*A*** aggregation. However, the degree to which one type of aggregation mechanism dominates over the other will vary considerably based on the content (availability) of vacancies and interstitials, which is related to the deformation and thermal growth history of the diamond (Hull and Bacon 1984; Fisher et al. 2009; Smit et al. 2018).

Data Availability

The *Caxbd_Inherit_2024-Ib* Excel spreadsheet for deconvoluting the N-region of the FTIR spectra of *Type Ib* + IaA diamonds and Online Materials[1] Appendix A (Sections A1 and A2; Figs A1–A7), Appendix B (Figs. B1–B16), and Appendix C (Tables C1 and C2) can be accessed online and from the University of Padova repository at https://researchdata.cab.unipd.it/id/eprint/1537. See also the Online Materials[1].

Acknowledgments and Funding

We thank Simon Kohn and an anonymous reviewer for their insightful and constructive comments, which greatly improved the manuscript. We also thank the associate editor, Suzette Timmerman, for handling this manuscript. This work was funded by the European Union (ERC, INHERIT, Starting Grant No.101041620). Views and opinions expressed are, however, those of the author(s) only and do not necessarily reflect those of the European Union or the European Research Council Executive Agency. Neither the European Union nor the granting authority can be held responsible for them.

References Cited

Ashfold, M.N.R., Goss, J.P., Green, B.L., May, P.W., Newton, M.E., and Peaker, C.V. (2020) Nitrogen in diamond. Chemical Reviews, 120, 5745–5794, https://doi.org/10.1021/acs.chemrev.9b00518.

Babich, Yu.V., Feigelson, B.N., and Chepurov, A.I. (2016a) Manifestation of nitrogen interstitials in synthetic diamonds obtained using a temperature gradient technique (Fe-Ni-C system). Geochemistry International, 54, 922–927, https://doi.org/10.1134/S0016702916100025.

——— (2016b) Distribution of H1a-centers in as-grown diamonds of Fe-Ni-C system: FTIR-mapping study. Diamond and Related Materials, 69, 8–12, https://doi.org/10.1016/j.diamond.2016.07.001.

Boyd, S.R., Kiflawi, I., and Woods, G.S. (1994) The relationship between infrared absorption and the A defect concentration in diamond. Philosophical Magazine B, 69, 1149–1153, https://doi.org/10.1080/01418639408240185.

Chrenko, R.M., Strong, H.M., and Tuft, R.E. (1971) Dispersed paramagnetic nitrogen content of large laboratory diamonds. Philosophical Magazine: A Journal of Theoretical Experimental and Applied Physics, 23, 313–318, https://doi.org/10.1080/14786437108216387.

Chrenko, R.M., Tuft, R.E., and Strong, H.M. (1977) Transformation of the state of nitrogen in diamond. Nature, 270, 141–144, https://doi.org/10.1038/270141a0.

Clark, C.D. and Davey, S.T. (1984) One-phonon infrared absorption in diamond. Journal of Physics C: Solid State Physics, 17, 1127.

Collins, A.T. (1980) Vacancy enhanced aggregation of nitrogen in diamond. Journal of Physics C: Solid State Physics, 13, 2641–2650, https://doi.org/10.1088/0022-3719/13/14/006.

——— (1982) Colour centres in diamond. The Journal of Geology, 18, 37–75.

Curtolo, A., Novella, D., Logvinova, A., Sobolev, N.V., Davies, R.M., Day, M.C., Pamato, M.G., and Nestola, F. (2023) Petrology and geochemistry of Canadian diamonds: An up-to-date review. Earth-Science Reviews, 246, 104588, https://doi.org/10.1016/j.earscirev.2023.104588.

Dale, M.W. (2015) Colour Centres on Demand in Diamond, 250 p. Ph.D. thesis, University of Warwick.

Davies, G., Lawson, S.C., Collins, A.T., Mainwood, A., and Sharp, S.J. (1992) Vacancy-related centers in diamond. Physical Review B: Condensed Matter, 46, 13157–13170, https://doi.org/10.1103/PhysRevB.46.13157.

Day, M.C., Pamato, M.G., Novella, D., and Nestola, F. (2023) Imperfections in natural diamond: The key to understanding diamond genesis and the mantle. La Rivista del Nuovo Cimento della Società Italiana di Fisica, 46, 381–471, https://doi.org/10.1007/s40766-023-00045-6.

Day, M.C., Jollands, M.C., Novella, D., Nestola, F., Dovesi, R., and Pamato, M.G. (2024) Hydrogen-related defects in diamond: A comparison between observed and calculated FTIR spectra. Diamond and Related Materials, 143, 110866, https://doi.org/10.1016/j.diamond.2024.110866.

Dischler, B. (2012) Handbook of Spectral Lines in Diamond, 480 p. Springer.

Dyer, H.B., Raal, F.A., Du Preez, L., and Loubser, J.H.N. (1965) Optical absorption features associated with paramagnetic nitrogen in diamond. Philosophical Magazine, 11, 763–774, https://doi.org/10.1080/14786436508230081.

Downloaded from pubs.geoscienceworld.org/msa/ammin/article-pdf/111/3/360/7778962/ammin-2025-9722.1.pdf by guest on 30 October 2026

Evans, T. and Qi, Z. (1982) The kinetics of the aggregation of nitrogen atoms in diamond. Proceedings of the Royal Society of London A: Mathematical and Physical Sciences, 381, 159–178, https://doi.org/10.1098/rspa.1982.0063.

Fisher, D. and Lawson, S.C. (1998) The effect of nickel and cobalt on the aggregation of nitrogen in diamond. Diamond and Related Materials, 7, 299–304, https://doi.org/10.1016/S0925-9635(97)00246-X.

Fisher, D., Sibley, S.J., and Kelly, C.J. (2009) Brown colour in natural diamond and interaction between the brown related and other colour-inducing defects. Journal of Physics: Condensed Matter, 21, 364213, https://doi.org/10.1088/0953-8984/21/36/364213.

Fritsch, E. and Delaunay, A. (2018) What truly characterises a chameleon diamond? An example of an atypical 25.85 ct stone. The Journal of Geology, 36, 142–151.

Fritsch, E., Scarratt, K., Collins, A.T., Messier, R., Glass, J.T., Butler, J.E., and Roy, R. (1991) Optical properties of diamonds with an unusually high hydrogen content. In Materials Research Society International Conference Proceedings. Second International Conference on New Diamond Science and Technology, pp. 23–27.

Gali, A., Lowther, J.E., and Deák, P. (2001) Defect states of substitutional oxygen in diamond. Journal of Physics Condensed Matter, 13, 11607–11613, https://doi.org/10.1088/0953-8984/13/50/319.

Goss, J.P., Coomer, B.J., Shaw, T.D., Briddon, P.R., Rayson, M., and Öberg, S. (2001) Self-interstitial aggregation in diamond. Physical Review B: Condensed Matter and Materials Physics, 63, 195208.

Goss, J.P., Jones, R., Heggie, M.I., Ewels, C.P., Briddon, P.R., and Öberg, S. (2002) Theory of hydrogen in diamond. Physical Review B: Condensed Matter, 65, 115207, https://doi.org/10.1103/PhysRevB.65.115207.

Goss, J.P., Coomer, B.J., Jones, R., Fall, C.J., Briddon, P.R., and Öberg, S. (2003) Extended defects in diamond: The interstitial platelet. Physical Review B: Condensed Matter, 67, 165208, https://doi.org/10.1103/PhysRevB.67.165208.

Goss, J.P., Briddon, P.R., Papagiannidis, S., and Jones, R. (2004) Interstitial nitrogen and its complexes in diamond. Physical Review B: Condensed Matter and Materials Physics, 70, 235208, https://doi.org/10.1103/PhysRevB.70.235208.

Goss, J.P., Briddon, P.R., Hill, V., Jones, R., and Rayson, M.J. (2014) Identification of the structure of the 3107 cm^{-1} H-related defect in diamond. Journal of Physics: Condensed Matter, 26, 145801, https://doi.org/10.1088/0953-8984/26/14/145801.

Graham, R.J., Moustakas, T.D., and Disko, M.M. (1991) Cathodoluminescence imaging of defects and impurities in diamond films grown by chemical vapor deposition. Journal of Applied Physics, 69, 3212–3218, https://doi.org/10.1063/1.348539.

Hainschwang, T. (2014) Diamants de type Ib: Relations entre les propriétés physiques et gemmologiques des diamants contenant de l'azote isolé. Ph.D. thesis, Université de Nantes.

Hainschwang, T., Notari, F., Fritsch, E., and Massi, L. (2006) Natural, untreated diamonds showing the A, B and C infrared absorptions ("ABC diamonds"), and the H2 absorption. Diamond and Related Materials, 15, 1555–1564, https://doi.org/10.1016/j.diamond.2005.12.029.

Hainschwang, T., Notari, F., Fritsch, E., Massi, L., Rondeau, B., Breeding, C.M., and Vollstaedt, H. (2008) HPHT treatment of CO_2 containing and CO_2-related brown diamonds. Diamond and Related Materials, 17, 340–351, https://doi.org/10.1016/j.diamond.2008.01.022.

Hainschwang, T., Fritsch, E., Notari, F., and Rondeau, B. (2012) A new defect center in type Ib diamond inducing one phonon infrared absorption: The Y center. Diamond and Related Materials, 21, 120–126, https://doi.org/10.1016/j.diamond.2011.11.002.

Hainschwang, T., Notari, F., and Pamies, G. (2020) A defect study and classification of brown diamonds with deformation-related color. Minerals, 10, 903, https://doi.org/10.3390/min10100903.

Hauri, E.H., Wang, J., Pearson, D.G., and Bulanova, G.P. (2002) Microanalysis of δ13C, δ15N, and N abundances in diamonds by secondary ion mass spectrometry. Chemical Geology, 185, 149–163, https://doi.org/10.1016/S0009-2541(01)00400-4.

Howell, D., O'Neill, C.J., Grant, K.J., Griffin, W.L., O'Reilly, S.Y., Pearson, N.J., Stern, R.A., and Stachel, T. (2012a) Platelet development in cuboid diamonds: Insights from micro-FTIR mapping. Contributions to Mineralogy and Petrology, 164, 1011–1025, https://doi.org/10.1007/s00410-012-0786-9.

Howell, D., O'Neill, C.J., Grant, K.J., Griffin, W.L., Pearson, N.J., and O'Reilly, S.Y. (2012b) μ-FTIR mapping: Distribution of impurities in different types of diamond growth. Diamond and Related Materials, 29, 29–36, https://doi.org/10.1016/j.diamond.2012.06.003.

Hull, D. and Bacon, D.J. (1984) Introduction to Dislocations, 272 p. Pergamon Press.

Humble, P. (1982) The structure and mechanism of formation of platelets in natural type Ia diamond. Proceedings of the Royal Society of London A: Mathematical and Physical Sciences, 381, 65–81, https://doi.org/10.1098/rspa.1982.0059.

Jones, R., Goss, J.P., Pinto, H., and Palmer, D.W. (2015) Diffusion of nitrogen in diamond and the formation of A-centres. Diamond and Related Materials, 53, 35–39, https://doi.org/10.1016/j.diamond.2015.01.002.

Kaminsky, F.V., Polyakov, V.B., Ber, B.Ya., Kazantsev, D.Yu., Khachatryan, G.K., and Shilobreeva, S.N. (2024) Hydrogen in natural diamond: Quantification of N3VH defects using SIMS and FTIR data. Chemical Geology, 661, 122185, https://doi.org/10.1016/j.chemgeo.2024.122185.

Kanda, H. and Watanabe, K. (1999) Distribution of nickel related luminescence centers in HPHT diamond. Diamond and Related Materials, 8, 1463–1469, https://doi.org/10.1016/S0925-9635(99)00070-9.

Kazuchits, V.N., Kazuchits, N.M., Rusetskiy, M.S., Korolik, O.V., Konovalova, A.V., and Ignatenko, O.V. (2021) Rapid HPHT annealing of synthetic IB-TYPE diamonds. Carbon, 174, 180–189, https://doi.org/10.1016/j.carbon.2020.12.002.

Kiflawi, I. and Bruley, J. (2000) The nitrogen aggregation sequence and the formation of voidites in diamond. Diamond and Related Materials, 9, 87–93, https://doi.org/10.1016/S0925-9635(99)00265-4.

Kiflawi, I. and Lang, A.R. (1976) On the correspondence between cathodoluminescence images and X-ray diffraction contrast images of individual dislocations in diamond. Philosophical Magazine, 33, 697–701, https://doi.org/10.1080/14786437608221130.

Kiflawi, I., Mayer, A.E., Spear, P.M., Van Wyk, J.A., and Woods, G.S. (1994) Infrared absorption by the single nitrogen and A defect centres in diamond. Philosophical Magazine. B, 69, 1141–1147, https://doi.org/10.1080/01418639408240184.

Kiflawi, I., Mainwood, A., Kanda, H., and Fisher, D. (1996) Nitrogen interstitials in diamond. Physical Review B: Condensed Matter, 54, 16719–16726, https://doi.org/10.1103/PhysRevB.54.16719.

Kiflawi, I., Kanda, H., Fisher, D., and Lawson, S.C. (1997) The aggregation of nitrogen and the formation of A centres in diamonds. Diamond and Related Materials, 6, 1643–1649, https://doi.org/10.1016/S0925-9635(97)00207-0.

Kiflawi, I., Kanda, H., and Mainwood, A. (1998) The effect of nickel and the kinetics of the aggregation of nitrogen in diamond. Diamond and Related Materials, 7, 327–332, https://doi.org/10.1016/S0925-9635(97)00162-3.

Kupriyanov, I.N., Palyanov, Y.N., Kalinin, A.A., and Shatsky, V.S. (2020) Effect of HPHT Treatment on Spectroscopic Features of Natural Type Ib-IaA Diamonds Containing Y Centers. Crystals, 10, 378, https://doi.org/10.3390/cryst10050378.

Lai, M.Y. (2018) Spectroscopic Analysis of Yellow Diamonds. M.Sc. thesis, University of Alberta, Alberta.

Lai, M.Y., Breeding, C.M., Stachel, T., and Stern, R.A. (2020a) Spectroscopic features of natural and HPHT-treated yellow diamonds. Diamond and Related Materials, 101, 107642, https://doi.org/10.1016/j.diamond.2019.107642.

Lai, M.Y., Stachel, T., Breeding, C.M., and Stern, R.A. (2020b) Yellow diamonds with colourless cores – evidence for episodic diamond growth beneath Chidliak and the Ekati Mine, Canada. Mineralogy and Petrology, 114, 91–103, https://doi.org/10.1007/s00710-020-00693-0.

Lai, M.Y., Hardman, M.F., Eaton-Magaña, S., Breeding, C.M., Schwartz, V.A., and Collins, A.T. (2024) Spectroscopic characterization of diamonds colored by the 480 nm absorption band. Diamond and Related Materials, 142, 110825, https://doi.org/10.1016/j.diamond.2024.110825.

Lawson, S.C., Fisher, D., Hunt, D.C., and Newton, M.E. (1998) On the existence of positively charged single-substitutional nitrogen in diamond. Journal of Physics Condensed Matter, 10, 6171–6180, https://doi.org/10.1088/0953-8984/10/27/016.

Liggins, S. (2010) Identification of point defects in treated single crystal diamond, 241 p. Ph.D. thesis, University of Warwick.

Liggins, S., Newton, M.E., Goss, J.P., Briddon, P.R., and Fisher, D. (2010) Identification of the dinitrogen (001) split interstitial H1a in diamond. Physical Review B: Condensed Matter and Materials Physics, 81, 085214, https://doi.org/10.1103/PhysRevB.81.085214.

Luo, Y. and Breeding, C.M. (2013) Fluorescence produced by optical defects in diamond: Measurement, characterization, and challenges. Gems & Gemology, 49, 82–97, https://doi.org/10.5741/GEMS.49.2.82.

Mainwood, A. (1994) Nitrogen and nitrogen-vacancy complexes and their formation in diamond. Physical Review B: Condensed Matter, 49, 7934–7940, https://doi.org/10.1103/PhysRevB.49.7934.

Mainwood, A., Larkins, F.P., and Stoneham, A.M. (1978) The structure and motion of the self-interstitial in diamond. Solid-State Electronics, 21, 1431–1433, https://doi.org/10.1016/0038-1101(78)90220-4.

Mashkovtsev, R.I., Rakhmanova, M.I., and Zedgenizov, D.A. (2021) Specific spectroscopic features of yellow cuboid diamonds from placers in the north-eastern Siberian Platform. Journal of Geosciences (Prague), 66, 117–126, https://doi.org/10.3190/jgeosci.323.

Massi, L. (2006) Etudes des defauts dans les diamants bruns et les diamants riches en hydrogene. Ph.D. thesis, University of Nantes.

Massi, L., Fritsch, E., Collins, A.T., Hainschwang, T., and Notari, F. (2005) The "amber centres" and their relation to the brown colour in diamond. Diamond and Related Materials, 14, 1623–1629, https://doi.org/10.1016/j.diamond.2005.05.003.

Mendelssohn, M.J. and Milledge, H.J. (1995) Geologically significant information from routine analysis of the mid-infrared spectra of diamonds. International Geology Review, 37, 95–110, https://doi.org/10.1080/00206819509465395.

Mineeva, R.M., Zudina, N.N., Titkov, S.V., Ryabchikov, I.D., Speransky, A.V., and Zudin, N.G. (2013) EPR spectroscopy of cubic diamonds from placers in the north-east of the Siberian platform: New type of nitrogen centers. Doklady Earth Sciences, 448, 243–247, https://doi.org/10.1134/S1028334X13020190.

Downloaded from pubs.geoscienceworld.org/msa/ammin/article-pdf/111/3/360/7778962/ammin-2025-9722.1.pdf by guest on 30 October 2026

Nadolinny, V.A., Yelisseyev, A.P., Baker, J.M., Twitchen, D.J., Newton, M.E., Feigelson, B.N., and Yuryeva, O.P. (2000) Mechanisms of nitrogen aggregation in nickel- and cobalt-containing synthetic diamonds. Diamond and Related Materials, 9, 883–886, https://doi.org/10.1016/S0925-9635(99)00356-8.

Nadolinny, V.A., Shatsky, V.S., Yuryeva, O.P., Rakhmanova, M.I., Komarovskikh, A.Yu., Kalinin, A.A., and Palyanov, Yu.N. (2020) Formation features of N3V centers in diamonds from the Kholomolokh placer in the Northeast Siberian Craton. Physics and Chemistry of Minerals, 47, 4, https://doi.org/10.1007/s00269-019-01070-w.

Nadolinny, V.A., Palyanov, Y.N., Borzdov, Y.M., Rakhmanova, M.I., Komarovskikh, A.Y., and Yurjeva, O.P. (2024) HTHP treatment of diamonds containing N1 centers. Neutral state of the N1 center as a limiting step in the aggregation of substitutional nitrogen into A form. Diamond and Related Materials, 141, 110632, https://doi.org/10.1016/j.diamond.2023.110632.

Nestola, F., Prencipe, M., Nimis, P., Sgreva, N., Perritt, S.H., Chinn, I.L., and Zaffiro, G. (2018) Toward a robust elastic geobarometry of kyanite inclusions in eclogitic diamonds. Journal of Geophysical Research: Solid Earth, 123, 6411–6423, https://doi.org/10.1029/2018JB016012.

Peaker, C. V., Goss, J.P., Briddon, P.R., Horsfall, A.B., and Rayson, M.J. (2015) Di-nitrogen-vacancy-hydrogen defects in diamond: a computational study. physica status solidi (a), 212, 2616–2620.

Reutsky, V.N., Shiryaev, A.A., Titkov, S.V., Wiedenbeck, M., and Zudina, N.N. (2017) Evidence for large scale fractionation of carbon isotopes and of nitrogen impurity during crystallization of gem quality cubic diamonds from placers of North Yakutia. Geochemistry International, 55, 988–999, https://doi.org/10.1134/S001670291711009X.

Robert, R., John, J.F., and Martin, A.E. (1933) Two types of diamond. Philosophical Transactions of the Royal Society of London Series A: Containing Papers of a Mathematical or Physical Character, 232, 463–535, https://doi.org/10.1098/rsta.1934.0013.

Salustro, S., Pascale, F., Mackrodt, W.C., Ravoux, C., Erba, A., and Dovesi, R. (2018) Interstitial nitrogen atoms in diamond. A quantum mechanical investigation of its electronic and vibrational properties. Physical Chemistry Chemical Physics, 20, 16615–16624, https://doi.org/10.1039/C8CP02484G.

Satoh, S., Sumiya, H., Tsuji, K., and Yazu, S. (1990) Difference in nitrogen concentration and aggregation among (111) and (110) growth sectors of large synthetic diamonds. In S. Saito, O. Fukunaga, and M. Yoshikawa, Eds., Science and Technology of New Diamond, p. 351–355. Terra Scientific Publishing.

Shatsky, V.S., Zedgenizov, D.A., Ragozin, A.L., and Kalinina, V.V. (2014) Carbon isotopes and nitrogen contents in placer diamonds from the NE Siberian craton: Implications for diamond origins. European Journal of Mineralogy, 26, 41–52, https://doi.org/10.1127/0935-1221/2013/0025-2347.

Smit, K.V., Shirey, S.B., and Wang, W. (2016) Type Ib diamond formation and preservation in the West African lithospheric mantle: Re-Os age constraints from sulphide inclusions in Zimmi diamonds. Precambrian Research, 286, 152–166, https://doi.org/10.1016/j.precamres.2016.09.022.

Smit, K.V., D'Haenens-Johansson, U.F.S., Howell, D., Loudin, L.C., and Wang, W. (2018) Deformation-related spectroscopic features in natural Type Ib-IaA diamonds from Zimmi (West African craton). Mineralogy and Petrology, 112, 243–257, https://doi.org/10.1007/s00710-018-0587-6.

Smit, K.V., Stachel, T., Luth, R.W., and Stern, R.A. (2019) Evaluating mechanisms for eclogitic diamond growth: An example from Zimmi Neoproterozoic diamonds (West African craton). Chemical Geology, 520, 21–32, https://doi.org/10.1016/j.chemgeo.2019.04.014.

Speich, L. and Kohn, S.C. (2020) QUIDDIT - Quantification of infrared active defects in diamond and inferred temperatures. Computers & Geosciences, 144, 104558, https://doi.org/10.1016/j.cageo.2020.104558.

Speich, L., Kohn, S.C., Wirth, R., Bulanova, G.P., and Smith, C.B. (2017) The relationship between platelet size and the B′ infrared peak of natural diamonds revisited. Lithos, 278-281, 419–426, https://doi.org/10.1016/j.lithos.2017.02.010.

Stachel, T. and Harris, J.W. (2009) Formation of diamond in the Earth's mantle. Journal of Physics: Condensed Matter, 21, 364206, https://doi.org/10.1088/0953-8984/21/36/364206.

Stachel, T. and Luth, R.W. (2015) Diamond formation—Where, when and how? Lithos, 220-223, 200–220, https://doi.org/10.1016/j.lithos.2015.01.028.

Taylor, W.R., Jaques, A.L., and Ridd, M. (1990) Nitrogen-defect aggregation characteristics of some Australasian diamonds: Time-temperature constraints on the source regions of pipe and alluvial diamonds. American Mineralogist, 75, 1290–1310.

Taylor, W.R., Canil, D., and Judith Milledge, H. (1996) Kinetics of Ib to IaA nitrogen aggregation in diamond. Geochimica et Cosmochimica Acta, 60, 4725–4733, https://doi.org/10.1016/S0016-7037(96)00302-X.

Titkov, S.V., Shigley, J.E., Breeding, C.M., Mineeva, R.M., Zudin, N.G., and Sergeev, A.M. (2008) Natural-Color Purple Diamonds from Siberia. Gems & Gemology, 44, 56–64, https://doi.org/10.5741/GEMS.44.1.56.

Titkov, S.V., Shiryaev, A.A., Zudina, N.N., Sergeev, A.M., Ryabchikov, I.D., Speransky, A.V., and Zhikhareva, V.P. (2015a) The luminescent nature of orange coloration in natural diamonds: Optical and EPR study. Physics and Chemistry of Minerals, 42, 131–141, https://doi.org/10.1007/s00269-014-0705-x.

Titkov, S.V., Mineeva, R.M., Zudina, N.N., Zudin, N.G., and Solodova, Yu.P. (2015b) Defects in cubic diamonds from the placers in the northeastern Siberian platform: Results of IR microspectrometry. Russian Geology and Geophysics, 56, 354–362, https://doi.org/10.1016/j.rgg.2015.01.026.

Van Enckevort, W.J.P. and Visser, E.P. (1990) Photoluminescence microtomography of diamond. Philosophical Magazine B, 62, 597–614, https://doi.org/10.1080/13642819008215258.

Vasilev, E., Gubanov, N., and Zedgenizov, D. (2024) Point defects in coated diamonds. Diamond and Related Materials, 148, 111519, https://doi.org/10.1016/j.diamond.2024.111519.

Wood, J.O. (2020) An elusive impurity: Studying hydrogen in natural diamonds, 219 p. Ph.D. thesis, University of Bristol.

Woods, G.S. (1986) Platelets and the infrared absorption of type Ia diamonds. Proceedings of the Royal Society of London, Series A, 407.

Zaitsev, A.M. (2001) Optical Properties of Diamond, 520 p. Springer.

Zedgenizov, D., Reutsky, V., and Wiedenbeck, M. (2017) The carbon and nitrogen isotope characteristics of Type Ib-IaA cuboid diamonds from alluvial placers in the Northeastern Siberian Platform. Minerals, 7, 178, https://doi.org/10.3390/min7100178.

Zedgenizov, D., Bogush, I., Shatsky, V., Kovalchuk, O., Ragozin, A., and Kalinina, V. (2019) Mixed-habit Type Ib-IaA diamond from an udachnaya eclogite. Minerals, 9, 741, https://doi.org/10.3390/min9120741

Manuscript received December 16, 2024
Manuscript accepted March 26, 2025
Accepted manuscript online April 3, 2025
Manuscript Handled by Suzette Timmerman

Endnotes:

[1]Deposit item AM-26-39722. Online Materials are free to all readers. Go online, via the table of contents or article view, and find the tab or link for supplemental materials.

Downloaded from pubs.geoscienceworld.org/msa/ammin/article-pdf/111/3/360/7778962/ammin-2025-9722.1.pdf by guest on 30 October 2026